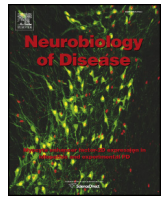




Contents lists available at ScienceDirect

Neurobiology of Disease

journal homepage: www.elsevier.com/locate/ynbdi

Q2 Novel therapeutic strategy for neurodegeneration by blocking A β seeding mediated aggregation in models of Alzheimer's disease

Q3 Simona Eleuteri^{a,b}, Saviana Di Giovanni^a, Edward Rockenstein^b, Mike Mante^b, Antony Adame^b,
Margarita Trejo^c, Wolf Wrasidlo^b, Fang Wu^d, Patrick C. Fraering^d, Eliezer Masliah^{b,d,*}, Hilal A. Lashuel^{a,**}

^a Laboratory of Molecular and Chemical Biology of Neurodegeneration, Brain Mind Institute, Station 19, School of Life Sciences, Ecole Polytechnique Fédérale de Lausanne (EPFL), CH-1015 Lausanne, Switzerland

^b Department of Neurosciences, School of Medicine, University of California at San Diego, La Jolla, CA 92093, USA

^c Department of Pathology, School of Medicine, University of California at San Diego, La Jolla, CA 92093, USA

^d Laboratory of Molecular and Cellular Biology of Alzheimer's Disease, Brain Mind Institute, Station 19, School of Life Sciences, Ecole Polytechnique Fédérale de Lausanne (EPFL), CH-1015 Lausanne, Switzerland

1 1 A R T I C L E I N F O

12 Article history:

13 Received 29 November 2013

14 Revised 14 July 2014

15 Accepted 10 August 2014

16 Available online xxxx

17 Keywords:

18 Alzheimer's disease

19 A β seeding-mediated aggregation

20 A β -propagation

21 Amyloid protein

22 Drug discovery

23 Inhibitors

A B S T R A C T

A β accumulation plays a central role in the pathogenesis of Alzheimer's disease (AD). Recent studies suggest that the process of A β nucleated polymerization is essential for A β fibril formation, pathology spreading and toxicity. Therefore, targeting this process represents an effective therapeutic strategy to slow or block disease progression. To discover compounds that might interfere with the A β seeding capacity, toxicity and pathology spreading, we screened a focused library of FDA-approved drugs in vitro using a seeding polymerization assay and identified small molecule inhibitors that specifically interfered with A β seeding-mediated fibril growth and toxicity. Mitoxantrone, bithionol and hexachlorophene were found to be the strongest inhibitors of fibril growth and protected primary cortical neuronal cultures against A β -induced toxicity. Next, we assessed the effects of these three inhibitors in vivo in the mThy1-APPtg mouse model of AD (8-month-old mice). We found that mitoxantrone and bithionol, but not hexachlorophene, stabilized diffuse amyloid plaques, reduced the levels of A β ₄₂ oligomers and ameliorated synapse loss, neuronal damage and astrogliosis. Together, our findings suggest that targeting fibril growth and A β seeding capacity constitutes a viable and effective strategy for protecting against neurodegeneration and disease progression in AD.

© 2014 Elsevier Inc. All rights reserved.

Q5 Introduction

Evidence from genetics, neuropathology, biochemistry and animal model studies continues to suggest that amyloid β protein (A β) aggregation and amyloid formation play central roles in the initiation and progression of neurodegeneration in Alzheimer's disease (AD) (Hartley et al., 1999; McLean et al., 1999). However, the mechanisms by which these processes contribute to the pathogenesis of AD and the nature of the toxic species remain subjects of active investigation and debate. Genetic mutations (Goate et al., 1991; Lemere et al., 1996; Nilsberth et al., 2001) or changes in the neurons that result in the increased production of A β or enhanced fibril formation have been linked to early onset forms of AD (McLean et al., 1999; Kumar-Singh et al., 2006).

A β is produced as a result of sequential proteolytic cleavage of the amyloid precursor proteins by β - and γ -secretase (Selkoe, 2012) resulting in

the generation of A β peptides of variable lengths, with A β ₄₀ being the predominate species and A β ₄₂ being the most amyloidogenic and toxic form (Duyckaerts et al., 2009; Mucke et al., 2000). A β fibril formation occurs via multiple mechanisms involving primary and secondary nucleation events and involves the formation of on or off-pathway oligomers.

The nucleated polymerization mechanism (Fig. 1b) is characterized by a nucleation phase associated with the formation of assembly competent oligomers followed by a cooperative oligomer growth and fibril formation by monomer addition (Harper and Lansbury, 1997). Several oligomeric intermediates of different morphologies, including spherical, chain-like, and annular oligomers have been observed during A β fibril formation in vitro (Jan et al., 2010), (Fig. 1b) and similar structures were identified during post-mortem biochemical analysis of AD brains (Lemere et al., 1996; Lesne et al., 2006).

This process of A β fibril formation can be seeded and accelerated by the addition of preformed fibrils (Fig. 1b). The addition of a small amount of preformed fibrillar aggregates (seeds) eliminates the lag phase of A β aggregation and accelerates the fibrillization of monomeric A β in vitro and in vivo (Harper and Lansbury, 1997). The pathological relevance and consequences of this process remain subjects of intense debate and active investigation. We have recently shown that the

* Correspondence to: E. Masliah, Departments of Neurosciences and Pathology School of Medicine, MTF Bldg, UCSD, 9500 La Jolla, CA 92093, USA.

** Corresponding author.

E-mail addresses: emasliah@ucsd.edu (E. Masliah), hilal.lashuel@epfl.ch (H.A. Lashuel).

Available online on ScienceDirect (www.sciencedirect.com).

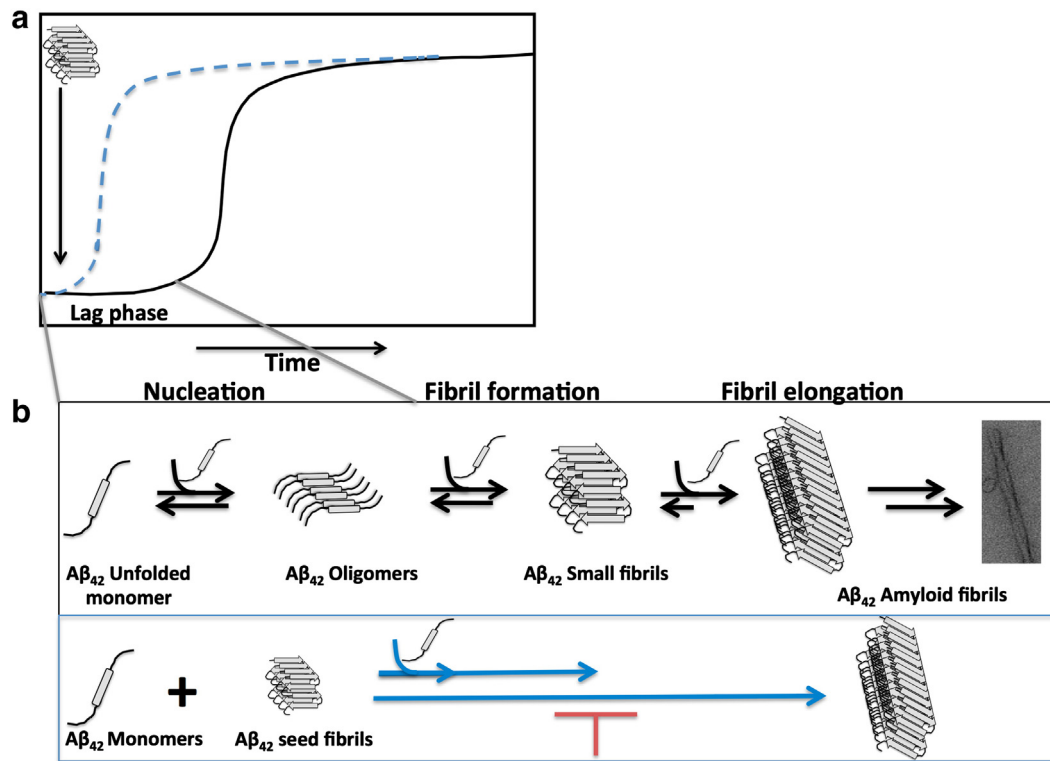


Fig. 1. The molecular basis of the nucleated polymerization high-throughput assay to identify inhibitors of fibril growth and seeding capacity. Fibril formation by A β follows a nucleated polymerization mechanism that is characterized by a nucleation phase associated with the formation of assembly competent oligomers followed by cooperative oligomer growth and fibril formation by monomer addition (a) 16. This process can be seeded and accelerated by the addition of preformed fibrils (b) and is thought to serve as the underlying mechanism for the spreading of A β pathology in the brain. The seeding polymerization assay we developed is based on adding a small amount of preformed fibrils to monomeric A β solutions and monitoring fibril growth in the presence or absence of small molecules. a) A schematic depiction of the kinetics of amyloid formation via a nucleated polymerization mechanism in the absence (in black) and presence (in blue) of preformed fibrillar seeds. b) The general mechanism of amyloid formation in vitro. The schematic depiction below illustrates the basis of our seeding polymerization assay to identify small molecules that interfere with fibril growth. The addition of small fibrils (seeds) eliminates the lag phase and accelerates amyloid formation in vitro (in blue).

77 toxicity of oligomeric A β preparations is enhanced by the addition of
 78 monomeric A β . These studies demonstrated a direct correlation between
 Q7 the ability of A β oligomers to convert into fibrils and increase
 80 A β toxicity, supporting the hypothesis that the process of fibril formation
 81 and growth is also a key mediator of A β -induced toxicity. Increasing
 82 evidence from in vivo studies also suggests that the seeding-mediated
 83 aggregation of A β proteins is essential for the formation of amyloid
 84 plaques (Walker et al., 2013), amyloid propagation and spreading
 85 via a prion-like mechanism (Frost and Diamond, 2010).

86 Previous in vivo studies have shown that inoculation of brain homogenates
 87 from the brain of AD patient or aged β APP transgenic mice into β APP
 88 transgenic mice accelerates A β deposition via a seeding mechanism
 89 (Kane et al., 2000; Meyer-Luehmann et al., 2006; Eisele et al., 2009).
 90 The amyloid-inducing activity of brain extracts was completely abolished
 91 by the A β -immunodepletion, by passive immunization of the β APPtg mouse
 92 host with antibodies or by treatments of the extracts with formic acid,
 93 demonstrating that A β is a pre-requisite for the in vivo seeding process
 94 (Kane et al., 2000; Meyer-Luehmann et al., 2006). Previous studies in
 95 different brain areas have also shown that A β aggregates spread from
 96 the site of the injection to more distal regions, and the spreading is
 97 consistent with normal age-related deposition in APPtg mouse hosts
 98 (Eisele et al., 2009). Recently, Prusiner and collaborators have shown
 99 that synthetic A β aggregates inoculated into young APPtg mice form
 100 A β deposits similar to the deposits induced by brain-derived A β
 101 aggregates (Sthor et al., 2012).

102 Together, these data suggest that seeding-mediated A β fibril formation
 103 deposition in vivo might be a key mediator in AD progression, and
 104 acting on this process could represent an effective therapeutic strategy
 105 to slow or block disease progression. Therefore, we sought to discover
 106 compounds that might interfere with seeding-mediated aggregation

and toxicity. Towards this goal, we screened an FDA-approved library
 of bioactive compounds, and sixteen molecules were identified as
 strong inhibitors of A β ₄₂ seeding-mediated aggregation. Three of these
 inhibitors exhibited the strongest inhibition on seeding-mediated
 aggregation and were shown to protect against A β -induced neuronal
 toxicity; these inhibitors were selected for validation in an AD animal
 model. Here, we show that the administration of two of these
 compounds two months after the initiation of A β deposition reduced
 A β accumulation and oligomer formation and protected against A β -
 induced synapse loss and neuronal damage.

Materials and methods

Preparation of the working compounds

A library containing 1040 small chemical compounds consisting of
 FDA-approved drugs was purchased from MicroSource Discovery System
 (Gaylordsville CT, USA). *N*-[*N*-(3,5-difluorophenylacetyl)-*L*-alanine]-(*S*)-
 phenylglycine-*t*-butyl ester (DAPT), egg yolk 1,2-Diacyl-*sn*-glycero-3-
 phosphocholine (PC) and 1,2-Diacyl-*sn*-glycero-3-phosphoethanolamine
 (PE) were purchased from Sigma-Aldrich (Steinheim, Germany).

Sample preparations for fibrillization studies and toxicity assays

Preparation and characterization of A β ₄₂ low molecular weight (LMW) and protofibril (PF)-A β ₄₂

A β ₄₂ was synthesized and purified by Dr. James I. Elliot at Yale University (New Haven, CT, USA). To prepare the monomeric A β ₄₂ stock solution (90% of monomers and LMW in equilibrium), the A β ₄₂ was dissolved in 6 M guanidine-HCl at a concentration of 1 mg/ml and

- 132 subsequently centrifuged at 6000 rcf for 5 min. To prepare the low molecular weight (LMW) and protofibril (PF) A β ₄₂ stock solution (250 μ M, 133 1 mg/ml), the lyophilized A β ₄₂ was dissolved in 5% DMSO and 2 M Tris base, pH 7.6; it was then subjected to low speed centrifugation at 134 3000 rcf for 5 min. A β ₄₂ LMW and PF stock solution were loaded onto 135 a gel filtration column (Superdex 75 HR 10/30 Amersham) previously equilibrated with 10 mM Tris buffer and then the fraction was separated 136 and eluted in 10 mM Tris buffer. The concentration of A β ₄₂ (LMW and PF) was calculated using the theoretical molar extinction coefficient at 137 280 nm (1490 M⁻¹ cm⁻¹). To perform aggregation studies, A β ₄₂ was incubated at 37 °C in 1.5 ml polypropylene sterile tubes, with and without 138 different concentrations of inhibitors, at molar ratios of A β ₄₂: inhibitor of 1:0.5 and 1:2 for 48 h. 139
- 140 **Q8** *Preparation of A β ₄₂ seeds*
- 141 The A β ₄₂ seeds were prepared by the incubation of the A β ₄₂ solution (5% DMSO, 2 M Tris buffer, pH 7.6) at 37 °C under agitation for 72 h. 142 After three days of incubation, the fibrils were mechanically fragmented to yield a narrow distribution of smaller fibrillar structures (100–300-nm long) by ultra-sonication on ice using a SONICS Vibra Cell™ 143 equipped with a fine tip (20 × 5 second pulses, amplitude of 40, output watts of 6). The sonicated fibrils were diluted in 10 mM Tris buffer, 144 pH 7.6. Seeds and monomeric A β ₄₂ were incubated for 2–3 h at 37 °C with continuous shaking, with and without inhibitors, in black polystyrene 384-well plates (Nunc, Thermo Scientific, USA). The concentration of the seeds and fibrils was calculated on the basis of monomer concentration (250 μ M).
- 145 *Characterization of the A β ₄₂ species*
- 146 All the A β ₄₂ species generated using the protocols above (monomers, protofibrils, fibrils and fibril seeds) were characterized by size exclusion chromatography, ThT, and TEM as previously described in Jan et al. (2010). 147
- 148 *Fibrillization studies*
- 149 *Seeding polymerization assay*
- 150 Polymerization of soluble A β ₄₂ with or without A β ₄₂ seeds was assayed as described in Di Giovanni et al. (2010). Initial studies were performed by incubating a solution of monomers (M) and seeds (S) at molar ratios of 10:2 and 10:4. The inhibitory activity of the 1040 FDA-approved drugs using the seeding fibrillization assay was determined using a Zephyr® Compact Liquid Handling Workstation (Caliper Life Science). The assay was initiated by adding 64 μ l of M and 8 μ l of S (10:4 μ M) to each well of black polystyrene 384-well plates (Nunc, USA). During the assay, the plates were kept at 4 °C to avoid aggregation of the protein solutions. A total of 8 μ l of the compound solutions dissolved in 1% DMSO was added to the reaction mixture so that the final concentration of the tested compounds was 10 μ M. The plates were incubated at 37 °C for 3 h under agitation. The kinetics of the fibrillization were monitored using the standard Thioflavin T (ThT) binding assay as described below. The assay was performed by processing the microplate collection of each compound in duplicate. Curcumin was used as a positive control, and the results are reported as the percent inhibition compared with control wells lacking the test compounds. 151
- 152 *Drug hit validation assays*
- 153 The hits from the seeding polymerization assay were validated for their ability to inhibit the fibrillization of monomeric or protofibrillar A β ₄₂ in standard 1.5-ml tubes. The time course of A β ₄₂ fibrillization was measured using a ThT fluorescence assay and TEM. 154
- 155 *ThT fluorescence assay*
- 156 For the seeding polymerization assay described above, an aliquot of 80 μ l of 10 μ M A β ₄₂ solutions, previously incubated at 37 °C in the absence or presence of compounds, was added to 10 μ l of 100 μ M ThT and 10 μ l of 50 μ M glycine buffer (pH 8.5). Fluorescence measurements were performed with a spectrofluorometer (Analyst™ AD 96-384, Bucher. Biotech. AG, Basel) at 25 °C using black polystyrene 384-well plates. The excitation wavelength was set to 450 nm, and emission was monitored at 485 nm. All measurements were performed in triplicate. 157
- 158 *TEM analysis*
- 159 The samples for TEM analysis were prepared by placement on a Formvar-carbon copper grid for 1 min before removing the excess solution. The grid was washed with 2 drops of distilled water and 1 drop of uranyl acetate before staining with 1% of fresh uranyl acetate for 30 s. The grids were analyzed using a Zeiss OM 10 electron microscope. 160
- 161 *Preparation of cell cultures and administration of A β ₄₂*
- 162 *Primary cortical neuronal cultures (P1)*
- 163 Primary cortical neuronal cultures were prepared from the neocortices of 1-day-old rats as previously described (Hartley et al., 1999). 164
- 165 Cortical hemispheres were isolated in Hank's balanced salt solution (HBSS, Invitrogen) and incubated in 0.1% papain (Sigma-Aldrich). After 10 min, the papain was removed, and the reaction was blocked using 30% fetal calf serum (FCS, Invitrogen). Individual cells were obtained by trituration (8×); the cells were then resuspended in NeuroBasal medium 1× (Invitrogen) supplemented with 0.5 mM B27 (Invitrogen), 200 mM l-glutamine (Invitrogen), 25 μ M Glutamax, 5% heat-inactivated FCS and 2% penicillin/streptomycin (Pen/Strep, Invitrogen). Cells were seeded at a density of 3.5 × 10⁵ cells on a Petri dish (3 × 10⁴ cells/cm²) in NeuroBasal medium supplemented with B27, 0.5 mM glutamine and 2% Pen/Strep. After 7 days in vitro (DIV), cortical neurons were exposed to an A β ₄₂ crude preparation, which contained a mixture of A β monomers, oligomers and protofibrils obtained by the incubation of ~1 mg/ml A β ₄₂ solution [5% DMSO, 2 mM Tris buffer (pH 7.6)]. 166
- 167 The neurons were exposed to a concentration of 40 μ M for 24 h or coincubated with the compounds at different concentrations as described in the Results. 168
- 169 *Cell viability analysis*
- 170 *MTT assay*
- 171 The viability of the cortical neuron cultures was evaluated using a thiazolyl blue (MTT) assay. The cells were incubated for 15 min at 37 °C; the dark crystals that formed after the incubation were dissolved in 0.1 M Tris–HCl buffer containing 5% Triton X-100, and the absorbance was read at 570 nm in a multiple spectrophotometric reader (Victor). All quantitative data are presented as the mean ± SE. 172
- 173 *Purification of γ -secretase and C100-Flag*
- 174 γ -Secretase was purified from S-20 cells as described previously (Cacquevel et al., 2008; Fraering et al., 2005). APP-C100-Flag, the recombinant APP-based protein substrate of γ -secretase, was overexpressed in *Escherichia coli* and purified using a Flag-specific M2 affinity resin (Sigma-Aldrich) (Cacquevel et al., 2008; Fraering et al., 2005). 175
- 176 *γ -Secretase activity assays*
- 177 In vitro γ -secretase assays using the recombinant APP-C100-Flag substrate and purified γ -secretase were performed as previously described (Cacquevel et al., 2008; Fraering et al., 2005). Briefly, γ -secretase solubilized in 0.2% (wt/vol) CHAPSO-HEPES (pH 7.5) was incubated at 37 °C for 4 h with 1 mM APP-C100-Flag substrate, 0.1% (wt/vol) PC, 0.025% PE and 10 mM of bithionol, hexachlorophene or mitoxantrone. All compounds were added to the reactions from DMSO 178

249 stock solutions before the addition of APP-C100-Flag. After 4 h of incubation at 37 °C, the reactions were halted by adding the Laemmli sample buffer for western blot analyses. The resulting products, APP intracellular domain (AICD)-Flag and A β , were detected with a Flag-specific M2 antibody (1:1000; Sigma-Aldrich) and an A β -specific 6E10 antibody (1:1000; Covance), respectively (Cacquevel et al., 2008; Fraering et al., 2005).

256 Pharmacokinetics and brain distribution

257 For this purpose, the compounds were submitted to Sai Life Sciences Limited (Pune, India) for determination of compound levels in mouse plasma and brain samples after a single administration of 10 mg/kg. C57/BL6 mice (n = 3 per time point) were treated, and blood and brain samples were collected at 0, 0.08, 0.25, 0.5, 1, 2, 4, 8 and 24 h.

Q11 Compound levels were determined using LC-MS/MS pharmacokinetic parameters and calculated using a non-compartmental analysis tool of Q12 Phoenix WinNonlin (vs. 6.3).

265 APP transgenic mouse model

266 To perform in vivo studies, we used the previously described transgenic mouse model of AD (line 41) expressing hAPP751 cDNA containing the London (V717I) and Swedish (K670M/N671I) mutations under the regulatory control of the murine (m) Thy-1 gene (mThy1-hAPP751) (Rockenstein et al., 2001, 2002); female mice were used.

271 The rationale behind using only female mice in our project is that the distribution of plaques in these animals correlates with that observed in cortical areas of female AD patient (Kraszpulski et al., 2001). Gender-dependent elevated plaque formation has been reported in several APP transgenic mouse models: APP23 (Sturchler-Pierrat and Staufenbiel, 2000) and APP/Tau double transgenic mice (Lewis et al., 2001).

277 The female APPtg mice (8 months old) were treated with PBS (as the control) or bithionol, mitoxantrone or hexachlorophene. Bithionol and mitoxantrone, which are able to cross the brain–blood barrier (BBB), were administered to APPtg mice via a daily intraperitoneal injection for 1 month at different concentrations (bithionol, 10 mg/kg; mitoxantrone, 1 mg/kg). Hexachlorophene is unable to cross the BBB; thus, it was injected into the APPtg mouse brain via a cannula and an osmotic pump implanted into the right hemi ventricle (–1.0, 1.0, –3.0).

285 Brain tissue preparation and fractionation

286 The posterior mouse brain samples were homogenized in a sucrose-containing buffer (Buffer A) and separated into cytosolic and membrane fractions. The samples (0.1 g) were fractionated in 0.9 ml of Buffer A (containing PBS (pH 7.4), 0.32 M sucrose, 50 mM HEPES, 25 mM MgCl₂, 0.5 mM DTT, 200 μ g/ml PMSF, 2 μ g/ml pepstatin A, 4 μ g/ml leupeptin and 30 μ g/ml benzamidine hydrochloride). To avoid protein degradation and dephosphorylation and preserve the mouse brain tissues (Pham et al., 2010), preparation and fractionation of the brain tissues was performed in the presence of protease and phosphatase inhibitor cocktails (Calbiochem, San Diego, CA, USA) as previously described in (Pham et al., 2010). The samples were first homogenized and centrifuged at 3000 rcf for 5 min at 4 °C. The supernatant was collected and re-centrifuged at 100,000 \times g for 1 h at 4 °C. After centrifugation, the supernatant (cytosolic fraction) was kept, and the pellet (membrane fraction) was re-suspended in 0.4 ml of Buffer A and re-homogenized. The membrane fraction was used to detect the A β oligomers. A BCA assay was used to determine the protein concentrations of the membrane fraction and cytosolic fraction samples.

Q15 294 295 296 297 298 299 300 301 302 303

304 Immunoblot analysis

305 Mouse proteins (25 or 10 μ g) in the membrane fraction were separated on precast NuPage 4–12% Bis–Tris Acetate gels (Invitrogen, Life

Technologies) and transferred to a nitrocellulose membrane (Whatman 307 protein nitrocellulose transfer membrane, 0.2 μ m, Millipore). The membrane was blocked using 5% bovine serum albumin (Sigma-Aldrich) dissolved in 0.1% PBS-Tween 20 and then incubated at room temperature for 1 h with agitation and blotted with the primary antibody overnight at 4 °C. In the subsequent day, the membrane was incubated with a secondary antibody conjugated to horseradish peroxidase (HRP) and developed in a Versa Doc gel imaging system (Bio-Rad, Hercules, CA, USA). The Quantity One software package (Bio-Rad) was used for densitometry analysis. The protein concentrations were normalized to β -actin (1:1000).

Antibodies

318 We analyzed the levels of A β oligomers in mouse brain tissues using an immunoblotting assay performed with the membrane fraction and probed with anti-A β antibodies 82E1 (mouse IBL; 1:1000, Minneapolis, MN, USA) and 6E10 (mouse monoclonal; 1:1000, Signet). We simultaneously analyzed the levels of a synaptic vesicle protein, postsynaptic density-95 (mouse; 1:1000, PSD95), which has been shown to correlate with levels of oligomers in the brain, as well as the pre-synaptic protein synaptophysin using the anti-synaptophysin protein 38 (SY38) antibody (mouse monoclonal; 1:1000, Abcam).

327 To analyze the neuronal structure, we used MAP-2 (MAP378 mouse monoclonal; 1:250, Millipore) and NeuN (mouse monoclonal; 1:1000, Millipore); GFAP was used for astrogliosis analysis (rabbit polyclonal 1:500, Millipore). To normalize the data, we used β -actin (mouse monoclonal antibody; 1:1000, Millipore).

Determination of A β _{1–42} levels using ELISA

334 Quantitative evaluation of A β ₄₂ in mouse brains was performed using a solid phase sandwich enzyme-linked immunosorbent Assay (ELISA; Human A β ₄₂ kit, Invitrogen). The quantification of A β _{1–42} by the ELISA kit was performed on mouse membrane fraction samples or in brain tissues fractionated in guanidine-HCl, as previously reported (Masliah et al., 2000).

Immunohistochemistry analysis

341 Immunohistochemistry analyses were performed as described previously (Masliah et al., 2001). Vibratome sections were immunolabeled using a mouse monoclonal antibody against A β (clone 82E1, 1:500), anti-MAP2, anti-synaptophysin (SYN, clone SY38, 1:20; Chemicon), anti-NeuN, or anti-GFAP (a marker for astroglial cells) and detected using fluorescein isothiocyanate-conjugated secondary antibodies (1:75; Vector Laboratories, Burlingame, CA, USA). The sections were processed simultaneously under the same conditions, and the experiments were performed twice to assess reproducibility. The FITC-labeled immunofluorescent sections were analyzed with the LSCM system (BioRad, Hercules, CA, USA), and the serial optical z-sections (0.2- μ m thick) were imaged with a Zeiss 63 \times (N.A. 1.4) objective on an Axiovert 35 microscope (Zeiss, Thornwood, NY, USA).

Immunocytochemical staining

354 Neurons were fixed with paraformaldehyde (4% diluted in sodium phosphate buffer 1 \times , pH 7.4) for 20 min. The sections were incubated with a primary antibody (anti-MAP2; 1:500) in a primary antibody solution (5% BSA in PBS-Tween 0.01%) overnight at 4 °C, and the cells were then washed and incubated with a secondary antibody conjugated to Alexa Fluor 488 for 1 h at room temperature. The coverslips were then washed in a fresh antibody solution. The neurons on coverslips were imaged with a Zeiss 63 \times (N.A. 1.4) objective on an Axiovert 35 microscope (Zeiss, Thornwood, NY, USA).

364 *Electron microscopy analysis of fibril formation in brain tissues*

365 The mouse brain tissues were also analyzed through TEM.
366 Vibratome sections were postfixed in 1% glutaraldehyde, treated with
367 osmium tetroxide, embedded in epon araldite and sectioned with an
368 ultramicrotome (Leica, Nussloch, Germany). The grids were analyzed
369 with a Zeiss OM 10 electron microscope.

370 *Statistical analyses*

371 Statistical analyses were performed using the SPSS 12.0 software
372 package (SPSS Inc., Chicago, IL, USA). The Kolmogorov–Smirnov test
373 was used to check for normal distribution of the data, and t-tests were
374 applied to identify significant ($p < 0.05$) group differences. For multiple
375 comparisons, a one-way ANOVA with post-hoc Fisher tests was used. All
376 data proved to be normally distributed, and each experiment had a sam-
377 ple size of $N = 5$. For the IC_{50} calculation, we used the dose response
378 curves—inhibitors with variable slope and used [log] of the inhibitor
379 (the concentration of the inhibitors was in a range from 0.001 μM to
380 20 μM) and the data was analyzed by Prism.

381 **Results**

382 To identify molecules that specifically interfere with and block the
383 in vitro seeding mechanism (Fig. 1), we developed a robust seeding
384 fibrillization assay ($Z' = 0.87$) that is amenable to high-throughput
385 screening, as shown in Fig. 2a. To avoid artifacts due to the rapid aggre-
386 gation of $A\beta_{42}$, sample evaporation and inhomogeneous precipitation of
387 the protein, we optimized the aggregation conditions, and the
388 fibrillization of $A\beta_{42}$ monomers was complete within 2–3 h at low con-
389 centrations (5–10 μM) in the presence of a small amount of preformed
390 $A\beta_{42}$ fibrils (seeds, 1–2 μM). Fibrillar seeds of $A\beta_{42}$ were prepared by
391 fragmenting preformed and purified fibrils by sonication (Di Giovanni
392 et al., 2010). The extent of the $A\beta_{42}$ fibril formation was then assessed
393 using the Thioflavin T (ThT) fluorescence assay. The ThT signal of solu-
394 tions containing only monomers did not change over the 4-hour incuba-
395 tion, whereas samples containing 2 μM of preformed $A\beta$ fibrils showed a
396 marked increase in ThT fluorescence after a 2-hour incubation and
397 reached a maximum value within 4 h of incubation at 37 °C. The z factor
398 value was 0.87, thereby confirming the robustness of our assay.

399 Using this microplate-based $A\beta_{42}$ seeding and fibril growth assay,
400 we screened a library of 1040 compounds (80% of which are FDA-
401 approved) and identified 17 inhibitors of $A\beta_{42}$ fibril growth and seeding
402 capacity (Fig. 1a). These small molecules comprised three classes. The
403 first class consisted of aromatic phenolic or polyphenolic compounds,
404 the second class comprised heteroaromatic amines, and the third hybrid
405 contained structures with both phenolic and amine character com-
406 pounds. We then performed predicted drugability profiles of these com-
407 pounds based on the Lipinski rules, which included molecular mass,
408 lipophilicity (clogP) and topological polar surface areas (tpsa), and com-
409 puted the predicted blood–brain barrier (logBB) values. On the basis of
410 these analyses and after eliminating compounds with potential
411 toxiphoric groups, we selected 3 inhibitors (bithionol, mitoxantrone
412 and hexachlorophene; Fig. 2b) for validation in vitro and in an AD ani-
413 mal model.

414 *Validation and characterization of the hit compounds*

415 To validate the inhibitory effect on the seeding mechanism, different
416 concentrations of the compounds were added to a freshly prepared so-
417 lution of $A\beta_{42}$ obtained using Guanidine HCl 6 M. Fibrillar seeds at a final
418 concentration of 2 μM were then added, and the kinetics of fibrillization
419 were monitored through ThT fluorescence (Figs. 2c–e) and TEM
420 (Figs. 2f–j). In the absence of compounds, fibrillization proceeded im-
421 mediately to yield a dense network of amyloid fibrils, and the
422 fibrillization reaction was complete within 2 h (Figs. 2c–e). With

10 μM mitoxantrone (Fig. 2d), the seeding capacity of short fibrils was
423 abolished by more than 80–90%. Bithionol and hexachlorophene at the
424 same concentration showed an intermediate inhibitory effect of seeded
425 fibril growth of approximately 60–80% (Figs. 2c & e). Next, we assessed
426 the inhibitory effect of each compound on the seeded $A\beta_{42}$ fibril growth
427 at different concentrations, and the following IC_{50} values were obtained:
428 mitoxantrone, $IC_{50} = 1.7 \mu\text{M}$; bithionol, $IC_{50} = 5.33 \mu\text{M}$; and hexachlo-
429 rophene, $IC_{50} = 5.9 \mu\text{M}$. 430

The ability of these compounds to inhibit $A\beta_{42}$ growth and seeding
431 was also directly evaluated by TEM (Figs. 2f–j). Consistent with the
432 ThT data, 3 h of incubation with seeds and monomers resulted in the
433 formation of mature fibrils (Fig. 2g), whereas co-incubation with
434 bithionol (Fig. 2h), mitoxantrone (Fig. 2i) and hexachlorophene
435 (Fig. 2j) resulted in a significant inhibition of fibril growth and a reduc-
436 tion in the number of amyloid fibrils observed by TEM (Figs. 2c–e). Al-
437 though these findings suggest that these compounds are strong
438 inhibitors of $A\beta_{42}$ seeding capacity acting at a low molar ratio protein:
439 inhibitor, they do not rule out the possibility that they also influence
440 the aggregation of $A\beta_{42}$ by other mechanisms, notably, by stabilizing in-
441 termediates that precede the formation of mature fibrils or by altering
442 the aggregation pathway in favor of non-fibrillar or ThT-negative $A\beta_{42}$
443 aggregates. 444

To test these possibilities and determine the mode of action of the
445 three compounds, we investigated their capacity to inhibit the
446 fibrillization of monomeric and protofibrillar $A\beta_{42}$, which were freshly
447 prepared by size exclusion chromatography (SEC) as described previous-
448 ly (Di Giovanni et al., 2010). Fresh monomeric $A\beta_{42}$ solutions were incu-
449 bated (37 °C) with and without compounds at different molar ratios. The
450 compounds were co-incubated with monomeric or protofibrillar $A\beta_{42}$ at
451 two different molar ratios ($A\beta_{42}$:compound, 1:0.5 and 1:2) for 48 h
452 (Figs. 2k–m), and the extent of fibril formation was assessed through
453 ThT. Mitoxantrone was found to be the most active compound, showing
454 a greater than 80% inhibition of $A\beta_{42}$ fibrillization at 5–20 μM (Fig. 2l),
455 whereas bithionol and hexachlorophene exhibited inhibition in the
456 range of 80% (Figs. 2k & m), even at higher molar ratios (1:2, $A\beta_{42}$:com-
457 pound). Next, we assessed the inhibitory effect of each compound at dif-
458 ferent molar ratios of $A\beta_{42}$:inhibitor (range, 1:0.01–1:2), and the
459 following IC_{50} values were obtained: mitoxantrone, $IC_{50} = 2.5 \mu\text{M}$;
460 bithionol, $IC_{50} = 5.1 \mu\text{M}$; and hexachlorophene, $IC_{50} = 5 \mu\text{M}$. 461

To determine whether these compounds act by targeting aggrega-
462 tion intermediates on the amyloid pathway, we investigated their abil-
463 ity to inhibit the conversion of protofibrils into mature amyloid fibrils.
464 Mitoxantrone showed the strongest inhibition of protofibril to fibril
465 conversion (>80%, Fig. 2l), whereas bithionol and hexachlorophene
466 showed inhibition in the range of 50% (Figs. 2k & m). Given that these
467 compounds were identified as inhibitors of fibril growth, it is not sur-
468 prising that they were less effective at inhibiting protofibril growth.
469 Protofibrils are heterogeneous mixtures of $A\beta$ oligomers of different
470 sizes and morphology that are in dynamic equilibrium with the mono-
471 mers. Protofibrils lack the cross- β sheet structure that is characteristic of
472 amyloid fibrils and grow very slowly in the absence of excess mono-
473 mers. The strong inhibitory effects of the compounds observed in the
474 case of monomeric $A\beta$ could still be mediated by the inhibition of the
475 growth and seeding capacity during the early stages of fibril formation. 476

477 *Protection against $A\beta_{42}$ -induced toxicity in primary neuronal cultures*

To determine whether the inhibition of $A\beta$ growth and seeding ca-
478 pacity was sufficient to protect against $A\beta_{42}$ -induced toxicity, we inves-
479 tigated the neuroprotective properties of mitoxantrone, bithionol and
480 hexachlorophene against $A\beta_{42}$ -induced toxicity on newborn (P1) mice
481 cortical neurons (CNs) at 7 DIV as previously described (Sturchler-
482 Pierrat and Staufenbiel, 2000). First, we analyzed the effects of the
483 three compounds on the primary neurons. We found that bithionol
484 was not toxic to neurons (Fig. 3a). Mitoxantrone and hexachlorophene
485 showed a significant reduction of the cellular viability only at high
486

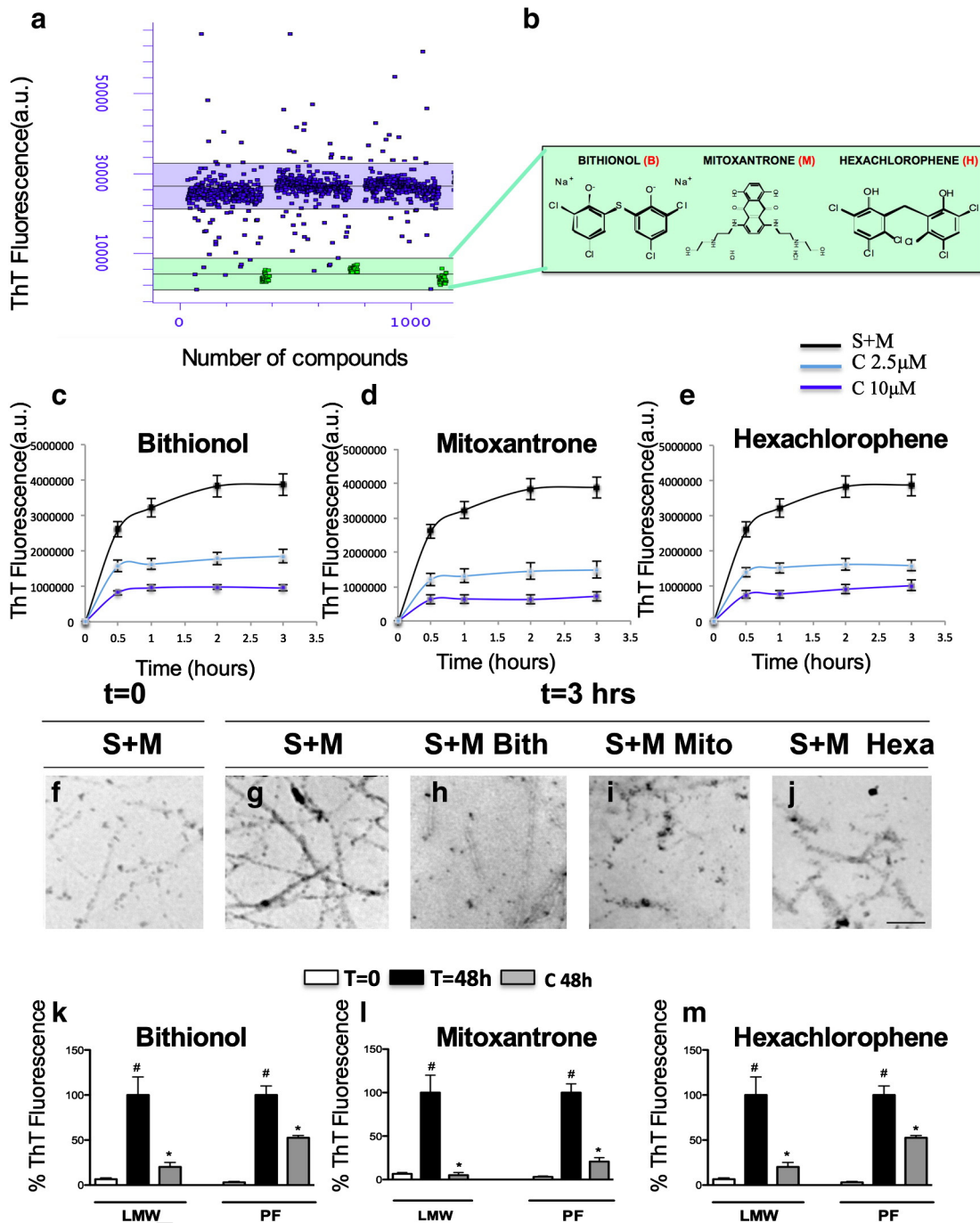


Fig. 2. Identification of new inhibitors of the A β ₄₂ seeding mechanism by high-throughput assay validation of inhibitory mechanisms on the seeding assay and on the LMW and PF elongation. **a**) Using a high-throughput assay, we screened an FDA-approved library (NINDS Custom Collection II) composed of 1040 bioactive compounds containing a diverse set of drugs, 85% of which are marketed drugs with a wide range of therapeutic usages including anti-inflammatory and analgesia use. The A β ₄₂ seeding polymerization assay was developed and optimized in 384-well plates, and a Z value of 0.869 was obtained by performing a ThT fluorescence assay using curcumin as a positive control. **b**) Identification of three strong inhibitors of the A β ₄₂ seeding mechanism: bithionol (B), mitoxantrone (M) and hexachlorophene (H) and the relative chemical structures (**b**). (**c–e**) In vitro analysis of the inhibitory effects of bithionol (**c**), mitoxantrone (**d**) and hexachlorophene (**e**) on the seeding mechanism evaluated by ThT. The A β ₄₂ peptide was incubated with the three compounds at a molar ratio of A β ₄₂:inhibitor (1:0.25 and 1:1), and the seeding reaction was monitored for 3 h using the ThT assay. (**f–j**) In vitro analysis of the inhibitory effects of bithionol (**c**), mitoxantrone (**d**) and hexachlorophene (**e**) on the seeding mechanism evaluated using a transmission electron microscope (TEM). (**k–m**) In vitro analysis of the inhibition of the bithionol (**k**), mitoxantrone (**l**) and hexachlorophene (**m**) on LMW and PF aggregation. The recombinant A β ₄₂ peptide was incubated with the compounds at molar ratios of A β ₄₂:inhibitor (1:0.5 and 1:1) at 37 °C for 48 h, and the aggregation state was evaluated using a ThT assay. (**i–m**) Structural analysis of the species stabilized after the inhibition has been performed by TEM after 3 h of the incubation of seeds (S) and monomers (M) (**j**), or with co-treatments of the compounds bithionol (**k**), mitoxantrone (**l**) and hexachlorophene (**m**) at a molar ratio of A β ₄₂:inhibitor (1:1).

487 concentrations (20 and 50 μ M; Figs. 3b–c). The primary neurons were 492
488 treated for 24 h with crude preparations of A β ₄₂ (40 μ M), which 493
489 contained predominantly monomeric and protofibrillar A β ₄₂ species 494
490 in the absence or presence of 0.5, 5 or 10 μ M of inhibitors (Di 495
491 Giovanni et al., 2010). Exposure of the neurons to 40 μ M of crude A β ₄₂

preparation reduced cellular viability by approximately 50–60% com- 492
pared with untreated CNs (Figs. 3d–f). However, A β ₄₂ cytotoxicity was 493
significantly reversed in the presence of low concentrations (5 and 494
10 μ M) of mitoxantrone or bithionol (Figs. 3d–e) in CNs. The 495
substoichiometric inhibition of A β toxicity is consistent with the 496

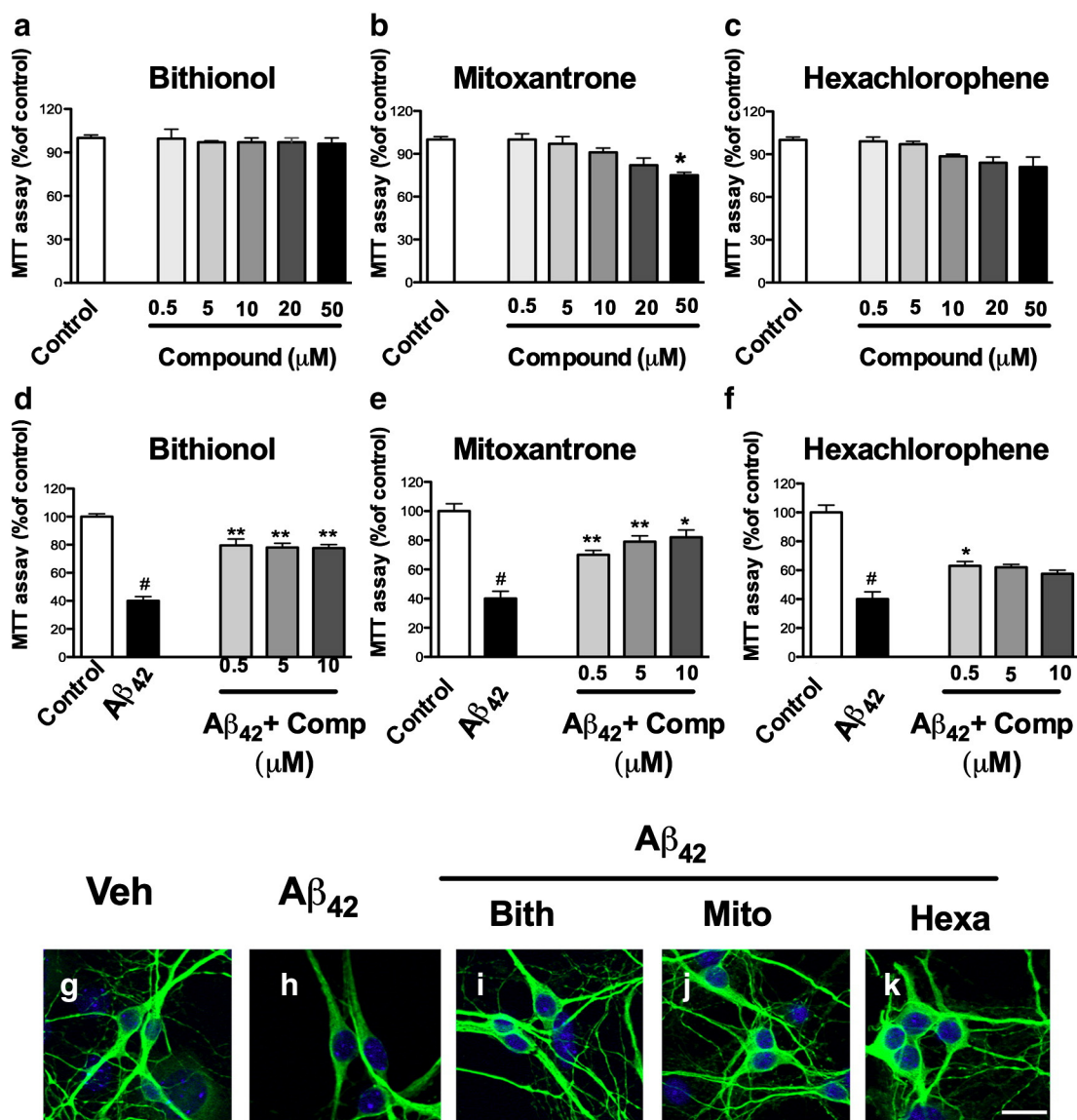


Fig. 3. Neuroprotection of the compounds against the A β ₄₂-induced toxicity in cortical neurons (CN). (a–b) Cortical neurons were treated with different concentrations of the compounds (0.5, 5, 10, 20 and 50 μ M) for 24 h. (d–f) The neurons were treated with 40 μ M of the crude preparation of A β ₄₂ or co-treated with the crude preparation and the compounds at different concentrations (0.5, 5 and 10 μ M) at 7 DIV. The effects of the compounds and the neuroprotection against the A β ₄₂-induced toxicity were evaluated using an MTT assay, and the control treatment was set to 100%. The error bars represent the mean \pm S.E. We used # to indicate the data compared to the control and * compared to the treatments with crude A β ₄₂ preparation, *p < 0.05, **p < 0.01. (g–k). The neuroprotection of the compounds against A β ₄₂-induced toxicity was evaluated by staining the neurons with MAP2 (green) by immunofluorescence, and the nuclei were stained with DAPI (blue).

497 proposed mode of actions of these compounds, i.e., that they target fibril
498 growth rather than stabilizing monomeric A β ₄₂. Despite the fact that
499 hexachlorophene was a stronger inhibitor of protofibrils to fibril con-
500 version and exhibited similar inhibitory effects on A β ₄₂ monomer
501 fibrillization, fibril growth and seeding capacity as bithionol, it showed
502 only modest protection against A β -induced toxicity in CNs (Fig. 3f).

503 To determine morphological changes in the CNs after the exposure to
504 the A β ₄₂ preparation and the neuroprotection of the compounds, we
505 performed immunolabeling for the neuronal cytoskeleton protein
506 MAP-2. Significant differences in MAP-2 staining were found between
507 control and A β ₄₂-exposed cells (Figs. 3g–k). We found dystrophic neu-
508 rons with several abnormal morphological features, including a dramatic
509 reduction in the neuronal network (Fig. 3h). The analysis of the MAP-2
510 immunoreactivity in neurons co-incubated with A β ₄₂ crude preparation
511 and compounds showed a significant reversion of the A β ₄₂-induced tox-
512 icity and a reduction of dystrophic neurites (Figs. 3i–k).

Bithionol and mitoxantrone reverse Alzheimer's disease features in APPtg mice 513 514

Motivated by the strong anti-amyloidogenic and neuroprotective properties observed for bithionol, mitoxantrone and hexachlorophene, we sought to validate our findings in an APP transgenic mouse model (APPtg). We first analyzed the plasma and brain pharmacokinetic properties of the three compounds. Following a single IV administration of each compound at 10 mg/kg, plasma and brain levels were determined by LC–MS/MS. For bithionol, the last AUC was 0.20 (20% brain penetration) with a half-life of 7.62 h in the plasma and 1.77 h in the brain. For mitoxantrone, the last AUC was 1.22 (100% brain penetration); the half-lives for plasma and brain were not determined. For hexachlorophene, the last AUC was 0.50 (50% brain permeability), and the half-lives were 4.4 h in the plasma and 5.64 h in the brain. After the brain and plasma levels of the three compounds were established, we analyzed

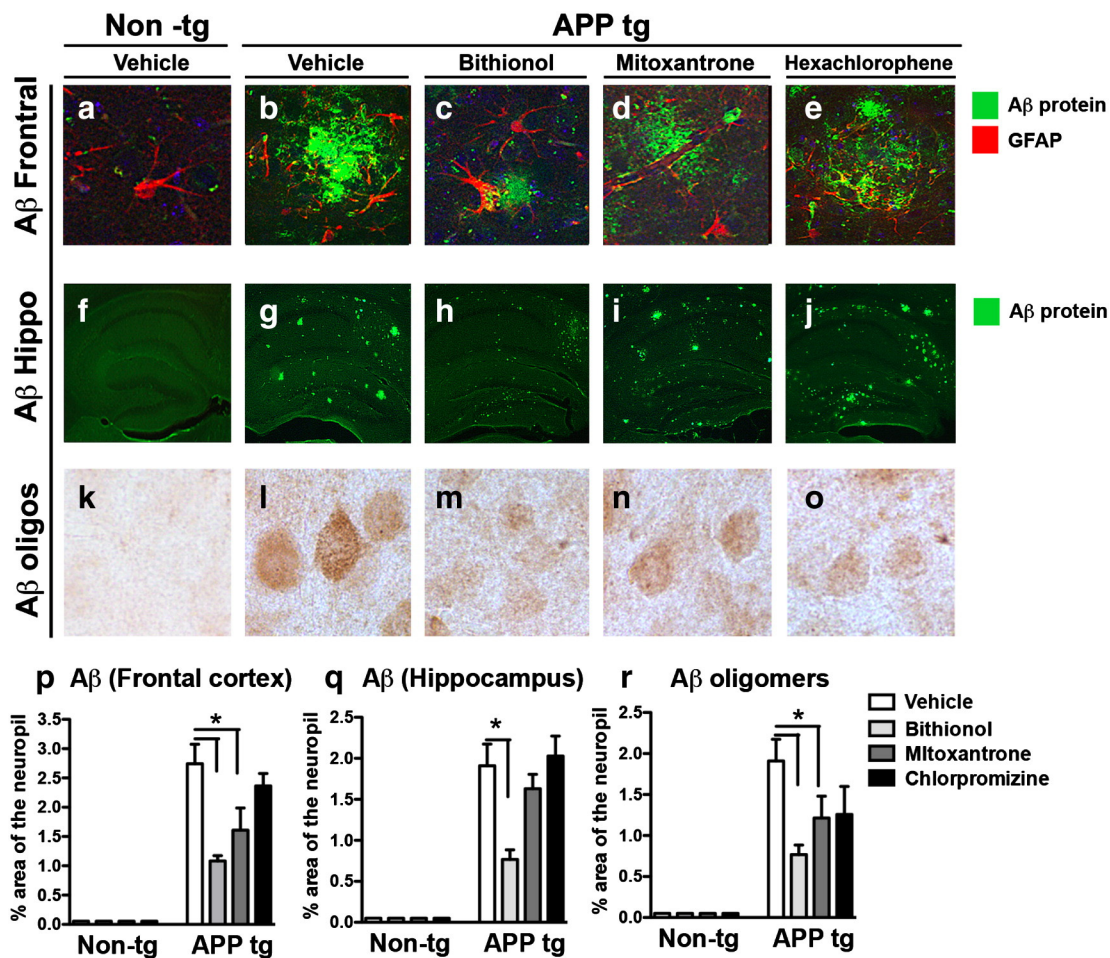


Fig. 4. Immunocytochemical analysis of the A β immunoreactivity in the frontal cortex and the hippocampus of APPtg mice to evaluate the effect of the treatments with bithionol, mitoxantrone and hexachlorophene. (a–j) Vibratome sections of the frontal cortex and the hippocampus were immunolabeled with thioflavine S, and plaques were analyzed in the frontal cortex and the hippocampus of the non-tg mice. (a–f) The APPtg mice (b–g) were compared with the diffuse plaque-like structures found in APPtg mice treated with bithionol (c–h) and mitoxantrone (d–i) or in more dense structures in the presence of hexachlorophene (c–j). (k–o) A β deposits in the frontal cortex were also evaluated using the 6E10 antibody; in the graphs (p–q), the data are related to a computer-aided quantitative analysis of the area of the neuropils covered (%) by the anti-A β antibody in the frontal cortex and the hippocampus' A β oligomers in non-tg and APPtg mice treated with the compounds. * $p < 0.05$ compared to APPtg mice by ANOVA with post-hoc Dunnett's test.

528 the effects of three inhibitors on the amyloid plaque features including
 529 A β_{42} deposits, A β_{42} oligomer levels, synapse loss, neuronal damage
 530 and astrogliosis, which together represent the neuropathological hall-
 531 marks of AD (7), in APPtg mice; the data were compared with the
 532 vehicle-treated APP transgenic (APP A β tg Vehicle) mice and the vehicle
 533 non-tg control (Non-tg Vehicle). To perform the *in vivo* studies, we used
 534 a transgenic mouse model that is characterized by the accumulation of
 535 mature plaques in the frontal cortex after 3–4 months of age and extends
 536 at 5–7 months of age, to the hippocampus, thalamus and olfactory
 537 regions. Moreover, the mice also produced high levels of the A β_{42} and
 538 exhibited synaptic damage and performance deficits in the water
 539 maze (Rockenstein et al., 2001, 2002). Bithionol and mitoxantrone
 540 cross the BBB and were administered to APPtg mice with a daily intra-
 541 peritoneal injection for 1 month at the respective concentrations of 10
 542 and 1 mg/kg. In contrast, hexachlorophene is unable to cross the BBB
 543 and was injected in the APPtg mouse brain via a cannula and osmotic
 544 pump implanted into the right hemi ventricle.

545 Diffuse-like plaque detection in APPtg brains treated with bithionol 546 and mitoxantrone

547 First, using immunostaining, we assessed the extent of A β_{42} accu-
 548 mulation and deposition into plaques in both APPtg mice (APPtg vehi-
 549 cle) and APPtg mice treated with the compounds in the frontal cortex
 550 (Figs. 4a–e) and the hippocampus (Figs. 4f–j). Subsequently, we

performed a quantitative analysis of the area of neuropils (%) covered
 551 by A β_{42} immunoreactivity in the frontal cortex (Fig. 4p) and the hippo-
 552 campus (Fig. 4q). Amyloid plaques are commonly classified as dense
 553 plaques surrounded by dystrophic neurites, reactive astrocytes, activa-
 554 ted microglial cells and synaptic loss, while diffuse plaques are usually
 555 non-neuritic and are not associated with synaptic loss (Mucke et al.,
 556 2000). In vehicle-treated APPtg mouse sections, we found plaques
 557 with a dense amyloid deposit morphology in both regions (Figs. 4b &
 558 g) and an increase of the A β_{42} immunoreactivity with respect to the
 559 control (Non-tg Vehicle); these findings were in agreement with a pre-
 560 vious analysis (Kumar-Singh et al., 2006). In APPtg mice treated with
 561 bithionol (Figs. 4c & h) and mitoxantrone (Figs. 4d & i), we observed
 562 diffuse-like plaques in the frontal cortex and the hippocampus and ob-
 563 served a significant decrease in the A β_{42} -immunoreactivity in the
 564 frontal cortex when compared with the APPtg mice for both compounds
 565 (Fig. 4p) and in the hippocampus for bithionol (Fig. 4q). In the APPtg
 566 mice treated with hexachlorophene (Figs. 4e & j), we detected dense
 567 plaques and high A β_{42} -immunoreactivity (Figs. 4p–q).
 568

Moreover, we analyzed the levels of A β plaques blotted with a 6E10
 569 antibody using DAB staining (Figs. 4k–o), thus confirming the ThS stain-
 570 ing of the plaques.
 571

Using electron microscopy, we also investigated the micrographs of
 572 neuropils and analyzed the status of synapses (SYN) and dendrites in con-
 573 trol mice, in vehicle-treated APP mice and in APP mice after the adminis-
 574 tration of bithionol, mitoxantrone and hexachlorophene (Figs. 5a–o). The
 575

576 neuropil electron micrographs are depicted in Figs. 5a–e. In the non-tg
 577 mice, the synapses and dendrites demonstrated normal characteristics
 578 and were well preserved (Fig. 5a), whereas in the vehicle-treated APPTg
 579 mice, abundant dystrophic neurites (DN) with electrodense bodies typi-
 580 cally associated with plaques were observed (Fig. 5b). In the bithionol-
 581 and mitoxantrone-treated APP mice (Figs. 5c–d), the axons were compa-
 582 rable to controls, while in the hexachlorophene-treated APP mice
 583 (Fig. 5e), abnormal dystrophic neurites were found. The neuropils with
 584 amyloid-containing areas were evaluated in Figs. 5f–o. No amyloid
 585 plaques were found in the non-tg mice (Figs. 5f & k). In the APP vehicle
 586 (Figs. 5g & l), there were abundant patches of amyloid fibrils (arrow-
 587 heads) forming plaques. In the bithionol and mitoxantrone groups, only
 588 few fibrillar aggregates were found scattered in the neuropils (Figs. 5h
 589 & m and i & n). In contrast, hexachlorophene APP-tg mice showed abun-
 590 dant fibrils and plaques (Figs. 5e & o).

591 Bithionol and mitoxantrone reduced the $A\beta_{42}$ intermediate species

592 The posterior parts of the mouse brains were fractionated by ultra-
 593 centrifugation, and the levels of $A\beta_{42}$ monomers and oligomers in the
 594 membrane fraction were detected through immunoblotting with an
 595 $A\beta_{42}$ antibody (82E1 clone). As shown in Fig. 6a, the immunoblot anal-
 596 ysis revealed different bands corresponding to $A\beta_{42}$ intermediate spe-
 597 cies. In agreement with previous studies (Pham et al., 2010), the
 598 analysis of the vehicle-treated APP transgenic brains displayed a signifi-
 599 cant increase in the levels of the bands corresponding to monomers and
 600 intermediate species (Fig. 6a) compared with the non-tg control. In con-
 601 trast, the treatment of the APPTg mice with bithionol and mitoxantrone
 602 induced a significant reduction in the levels of $A\beta_{42}$ monomers and in-
 603 termediate species (Figs. 6a–b). In the APPTg mice treated with hexa-
 604 chlorophene, the $A\beta_{42}$ level intermediate (Figs. 6a–b) was comparable
 605 to that observed in the vehicle-treated APPTg mice. To confirm the re-
 606 duction of the $A\beta_{42}$ levels in APPTg mice treated with bithionol and
 607 mitoxantrone, we quantified the $A\beta_{42}$ oligomers present in the brain

608 samples using ELISA; the $A\beta_{42}$ has already been identified as the most
 609 abundant species in the APPTg (line 41). We detected the $A\beta_{42}$ oligomers
 610 in membrane fractions (Fig. 6c) and simultaneously extracted the brain
 611 samples in guanidine-HCl to maximize the detection of total $A\beta_{42}$ levels
 612 (Fig. 6d). The administration of bithionol and mitoxantrone induced a
 613 significant and dramatic reduction in $A\beta_{42}$ levels compared with the
 614 vehicle-treated APPTg mice in both the membrane fractions and the
 615 guanidine-HCl brain extractions (Figs. 6c–d). In contrast, hexachloro-
 616 phene treatment did not significantly affect $A\beta_{42}$ levels. Together, the re-
 617 sults obtained through immunoblot analysis (Figs. 6a–b) and ELISA
 618 (Figs. 6c–d) confirmed a strong effect of bithionol and mitoxantrone
 619 on the reduction of $A\beta_{42}$ levels.

620 Bithionol and mitoxantrone neuroprotection against synapse loss and 621 neuronal damage

622 To evaluate the neuroprotective effects of bithionol and mitoxantrone
 623 against synapse loss in APPTg mice, we analyzed the levels of two
 624 proteins: synaptophysin, a major protein constituent of the membranes
 625 of pre-synaptic vesicles, and postsynaptic density-95 protein (PSD95).
 626 PSD95 levels have previously been correlated with the level of $A\beta$ oligo-
 627 mers in the brain, and reduced PSD95 protein levels have also been ob-
 628 served in AD patients and APPTg mice (Pham et al., 2010). We analyzed
 629 the levels of synaptophysin and PSD95 in vehicle-treated APPTg mice
 630 and in APPTg mice after the administration of bithionol, mitoxantrone
 631 and hexachlorophene through immunoblot analysis (Fig. 7a). In addition,
 632 we performed a semi-quantitative analysis of the bands through densi-
 633 tometry (Fig. 7b). The mouse brains were fractionated, and the mem-
 634 brane fractions were probed with anti-PSD95 and anti-SY38 antibodies.
 635 In agreement with previous studies in APPTg mice, we found a significant
 636 reduction of PSD95 and synaptophysin levels compared with the control
 637 and a significant reversion of the damage in the presence of the three
 638 compounds (Figs. 7a–b).

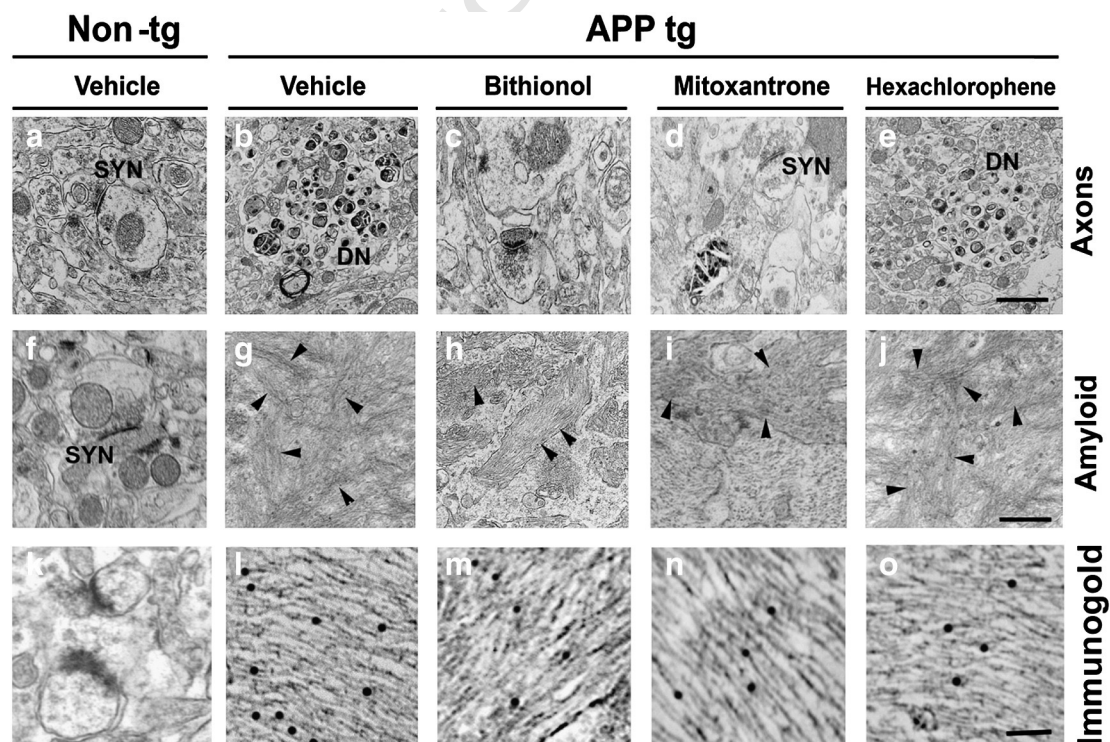


Fig. 5. The micrographs of the neuropil by EM; an analysis of the synapses (SYN) and dendritic status. Analysis of the control in vehicle-treated APP mice and in APP mice after the administration of bithionol, mitoxantrone and hexachlorophene. Analysis of the electron micrographs of the neuropil (a–e) in the non-tg mice (a), in the vehicle-treated APPTg mice (b), and in the bithionol-, mitoxantrone- and hexachlorophene-treated APP mice (c–e); analysis of the neuropil with the amyloid-containing areas (f–j) and of the amyloid-containing area by immunogold (k–o), in the non-tg mice (f & k), in the APP vehicle (g & l) and in the bithionol (h & m), mitoxantrone (i & n) and hexachlorophene (j & o)-treated APP-tg mice.

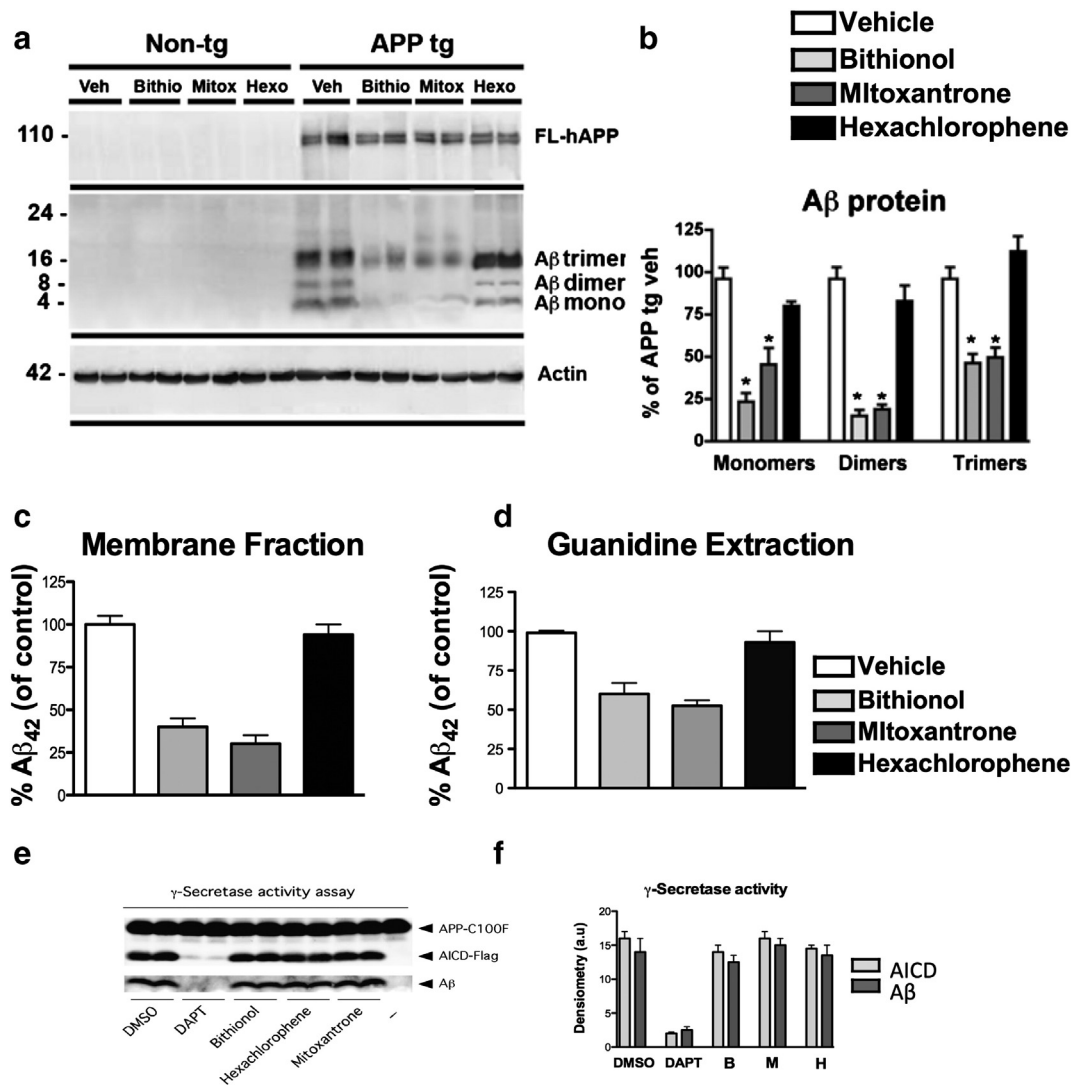


Fig. 6. Immunoblot analysis of A β species, ELISA test and γ -secretase activity in APPtg mice treated with bithionol, mitoxantrone and hexachlorophene. a) The mouse posterior brain tissues were homogenized in Buffer A, and the membrane fraction was probed with antibodies against A β (82E1) and β -actin. b) Semi-quantitative densitometric analyses of the bands representing A β monomers (4 kDa), dimers (8 kDa), and trimers (12 kDa). N = 5 cases per group. *p < 0.05 compared with APP/tg mice by ANOVA with post-hoc Dunnett's test. c) and d) Quantitative analysis of A β ₄₂ levels in APPtg mice treated with bithionol, mitoxantrone and hexachlorophene by ELISA. The quantification of A β ₄₂ levels in the membrane fraction (c) and guanidine-HCl extracted samples (d) N = 5 cases per group, female gender. *p < 0.05 compared with APPtg mice by ANOVA with post-hoc Dunnett's test. (e–f) The compounds do not affect the processing of APP-C100-Flag and A β production by purified γ -secretase. γ -Secretase solubilized in 0.2% CHAPSO-HEPES, pH 7.5, was incubated at 37 °C for 4 h with 1 μ M C100-Flag substrate, 0.1% PC, 0.025% PE and 10 μ M of bithionol, hexachlorophene and mitoxantrone. Activity assays included control reactions with 10 μ M of the γ -secretase inhibitor DAPT, DMSO (1.6% w/v) or a reaction with omitted γ -secretase (–). The reactions were halted by adding 0.5% SDS, and the resulting products were detected with anti-A β and -AICD-Flag antibodies 6E10 and M2, respectively. The relative levels of AICD-Flag or A β were estimated by densitometry (mean \pm SD; n = 2).

639 Moreover, to further investigate the neuroprotection of bithionol
 640 and mitoxantrone against synapse loss, we analyzed the levels of
 641 synaptophysin immunoreactivity in the frontal cortex (Figs. 7c–g) and
 642 hippocampus (Figs. 7h–m) of vehicle-treated APPtg mice (Figs. 7d & j)
 643 and mice treated with bithionol (Figs. 7e & k), mitoxantrone (Figs. 7f
 644 & l) and hexachlorophene (Figs. 7g & m). The non-tg mice were used
 645 as the control (Figs. 7c & h). In the frontal cortex and hippocampus of
 646 vehicle-treated APPtg mice, there was a progressive loss of SYN-IR
 647 (Figs. 7d & j) compared with the control. In contrast, APPtg mice treated
 648 with the compounds showed increased SYN-IR levels in both regions.
 649 We analyzed the neuroprotection in the brain samples treated with
 650 the compounds using a computer-aided quantitative analysis of the
 651 area (%) of neuropils covered by SYN-immunoreactivity terminals in
 652 the frontal cortex (Fig. 7n) and in the hippocampus (Fig. 7o). We
 653 found a significant reduction of synaptophysin immunoreactivity in
 654 APPtg mice treated with PBS compared with the controls in the frontal
 655 cortex (Figs. 7d & n) and in the hippocampus (Figs. 7j & o). The synapse
 656 loss in these two regions was significantly reversed in the presence of

bithionol (Figs. 7e, k & n–o), mitoxantrone (Figs. 7f & l and n–o) and
 658 hexachlorophene (Figs. 7g & m and n–o).

659 Moreover, we analyzed the effects of the compounds on the neuronal
 660 structure and integrity in the frontal cortex and hippocampus by immu-
 661 nostaining the mouse brain tissues for microtubule-associated protein 2
 662 (MAP2), which is a specific mature neuronal marker (Figs. 8a–j); we
 663 then quantified MAP2 immunoreactivity (Figs. 8k–l). In vehicle-treated
 664 APPtg mice, we found a loss of microtubule structures in the frontal cor-
 665 tex and the hippocampus (Figs. 8b & g) compared with the control
 666 (Figs. 8a & f), reflecting neuronal damage in these structures. This reduc-
 667 tion was confirmed by quantifying the MAP2-IR levels (Figs. 8k–l). In
 668 APPtg mice treated with bithionol, mitoxantrone and hexachlorophene,
 669 we found a reversion of the damage in the frontal cortex for the three
 670 compounds (Figs. 8c–e and k) as well as in the hippocampus when treat-
 671 ed with bithionol and mitoxantrone (Figs. 8h–i and l). Finally, we stud-
 672 ied the effects of the compounds on neuronal loss by evaluating NeuN
 673 immunoreactivity, a nuclear neuronal marker in the frontal cortex of
 674 APPtg mice (Figs. 8m–q and w) (McLean et al., 1999). In the brain

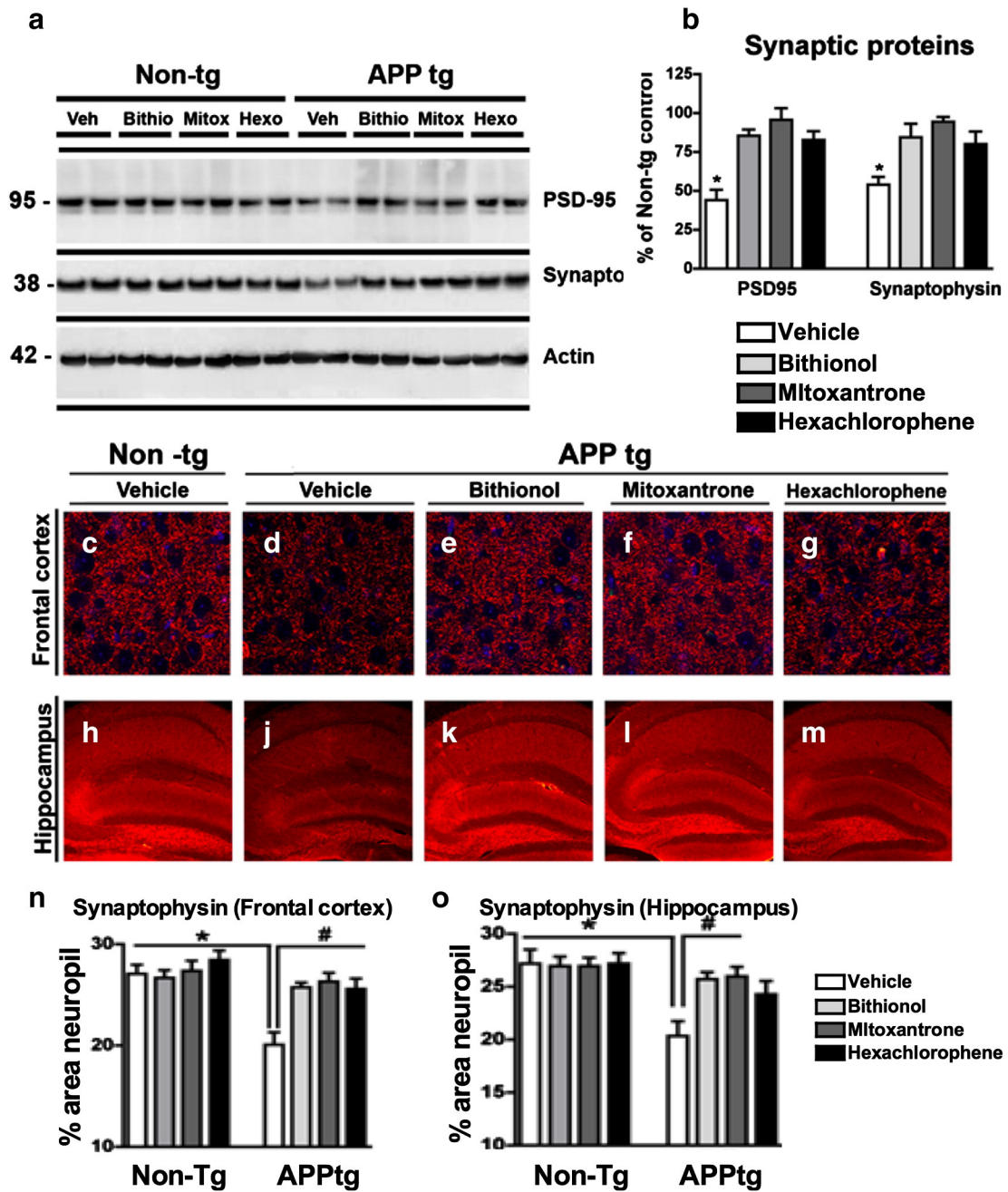


Fig. 7. Immunoblot analysis of the synaptic proteins (PSD95 and synaptophysin) and an analysis of the synaptophysin immunoreactivity in the frontal cortex and the hippocampus of APPtg mice treated with bithionol, mitoxantrone and hexachlorophene. **a**) Posterior brain tissues were homogenized in Buffer A, and the membrane fraction was probed with antibodies against PSD95 and synaptophysin (SY38). **b**) Semi-quantitative densitometric analyses of the bands for PSD95 and synaptophysin, $N = 5$ cases per group, $*p < 0.05$ compared with APP/tg mice by ANOVA with post-hoc Dunnett's test; **(c–m)** Sections of the frontal cortex (**c–g**) and the hippocampus (**h–m**) were immunolabeled with an anti-SYN antibody, a presynaptic terminal marker, and the nuclei are stained blue with DAPI; the brain sections were analyzed with the laser scanning confocal microscope to evaluate the protective effects of the compounds towards the synaptic damage. **(n–o)** Computer-aided quantitative analysis of % area of neuropil covered by SYN-immunoreactive terminals in the frontal cortex and the hippocampus of non-tg and APPtg mice treated with the compounds. $*p < 0.05$ compared with APPtg mice by ANOVA with post-hoc Dunnett's test.

675 sections of vehicle-treated APPtg mice, we found reduced NeuN immu-
 676 noreactivity (Fig. 8n), which was confirmed by cell counting (Fig. 8w
 Q21 compared with control in Fig. 8m). An increase in NeuN immunoreactiv-
 678 ity was found in APPtg mice treated with bithionol (Figs. 8o & w),
 679 mitoxantrone (Figs. 8p & w) and hexachlorophene (Figs. 8q & w).

680 *Bithionol and mitoxantrone protected neurons against astroglial reactivity*

681 Reactive astrogliosis is commonly associated with dense core
 682 plaques, indicating that amyloid- β is a major trigger of this glial re-
 683 sponse. To study the effects of the compounds against astroglial

reactivity, we analyzed the immunoreactivity of a glial marker, glial fi- 684
 brillar acidic protein (GFAP), in the frontal cortex (Figs. 8f–x). In control 685
 mouse sections, astrocytes were not reactive (Fig. 8r), and GFAP immu- 686
 noreactivity was very low (Fig. 8x). In vehicle-treated APPtg mice, the 687
 astrocytes exhibited an increase in the number of their intermediate fi- 688
 laments, changing their phenotypic appearance (Fig. 8s); an increase in 689
 the GFAP immunoreactivity was also observed (Fig. 8x). The treatment 690
 of APPtg mice with bithionol induced a strong and significant reduction 691
 of GFAP immunoreactivity (Fig. 8x). A significant effect on astroglial re- 692
 activity was also observed in animals treated with mitoxantrone 693
 (Figs. 8u & x) but not with hexachlorophene (Fig. 8r & x). Q22

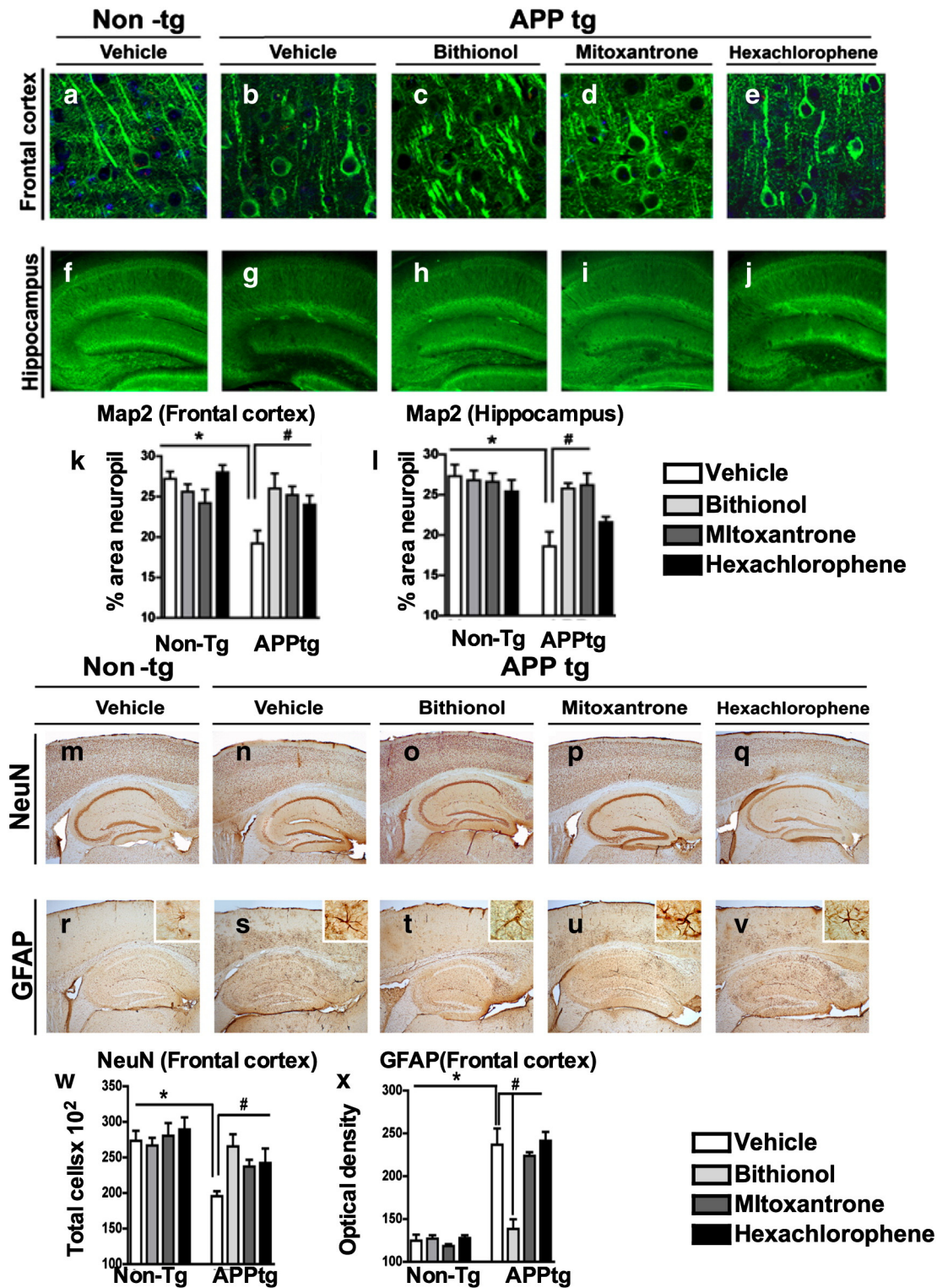


Fig. 8. Immunolabeling analysis for microtubule-associated protein 2 (MAP2), neuronal density and astrogliosis in the frontal cortex of APPtg mice treated with bithionol, mitoxantrone and hexachlorophene. Vibratome sections of the frontal cortex (a–e) and the hippocampus (f–j) were immunolabeled with an anti-MAP2 antibody, a neuronal-specific protein localized to the cytoskeleton, and the nuclei were stained by DAPI. The sections were visualized with the laser scanning confocal microscope (k–l). Computer-aided quantitative analysis of the area of neuropils (%) covered by MAP2 immunoreactivity. The effect of the compounds was also examined for neuronal density and astrogliosis using an antibody against the neuronal marker NeuN (m–q), and against the astrocytic marker GFAP (r–v). In the graphs (w–x), the analysis of the frontal cortex NeuN immunoreactivity and GFAP immunoreactivity across the experimental groups. * $p < 0.05$ compared with APPtg.

695 *Effects of the compounds on γ -secretase activity*

696 To determine whether the three selected compounds might influ-
697 ence A β production by altering the levels of secretases or by acting as

direct γ -secretase inhibitors, we investigated the ability of these com- 698
pounds to inhibit γ -secretase activity in a cell-free γ -secretase assay 699
performed with highly purified γ -secretase and APP-C100-Flag, a re- 700
combinant APP-based substrate (Cacquevel et al., 2008; Fraering et al., 701

2005). We did not observe any significant changes in secretase levels (Figs. 6e–f). Furthermore, and in contrast to the control γ -secretase inhibitor DAPT, none of the compounds tested at a final concentration of 10 μ M inhibited the γ -secretase-dependent processing of APP-C100-Flag or the production of both AICD and A β (Fig. 9). Together, our results demonstrate that bithionol, hexachlorophene and mitoxantrone do not target the γ -secretase-dependent processing of APP-C99 and A β production.

710 Discussion

711 Recently, we and others have shown that nucleated polymerization and seeding-mediated aggregation are essential for amyloid toxicity (Jan et al., 2010), progressive neurodegeneration and pathology spreading by several amyloid forming proteins (Jucker and Walker, 2011) including A β (Aguzzi et al., 2007; Langer et al., 2011; Lee et al., 2010), α -synuclein (Luk et al., 2012; Volpicelli-Daley et al., 2011) and IAPP (Gurlo et al., 2010). These findings have significant implications for the development of effective treatments to slow AD progression, especially because a significant amount of amyloid plaques is present in the brains of AD patients at the time of diagnosis. Amyloid formation, a nucleated polymerization process (Supplemental Fig. S1), is significantly accelerated by the presence or addition of preformed fibrils (Harper and Lansbury, 1997). Therefore, once significant amyloids have formed, preventing further aggregation and the spreading of the pathology becomes more challenging because the energetic barriers associated with the nucleation of aggregation are significantly lower, and further aggregation can occur below the critical concentration required for aggregation in the absence of a seed.

729 We hypothesized that inhibiting oligomer and seeding-mediated aggregation constitutes a viable and effective strategy for protecting against neurodegeneration and disease progression in AD. Unlike monomeric A β , which is unstructured and difficult to target using small molecules, A β oligomers and fibrils in particular are highly structured and possess hydrophobic pockets that can be targeted by small molecules (Autiero et al., 2013).

736 To test this hypothesis, we utilized an in vitro, cell-free high-throughput screening method to identify novel inhibitors of the A β ₄₂ seeding capacity and fibril growth. Specifically, bithionol, mitoxantrone and hexachlorophene were selected as potent inhibitors of the in vitro seeding-mediated aggregation. Of the three compounds, bithionol and mitoxantrone were the most effective at blocking A β pathology in APPtg mice, even when administered to an AD animal model 2–3 months after amyloid deposition. In addition, we found that these compounds were able to block the conversion of the monomers and protofibrils into mature fibrils by stabilizing oligomeric intermediates in the amyloid pathway. Stabilization of intermediate species with bithionol, mitoxantrone and hexachlorophene also reduced A β ₄₂-induced toxicity in primary cortical neurons.

749 After demonstrating that these compounds can prevent seeding-mediated fibril growth and protect neurons from A β -induced toxicity, we tested the inhibitors in vivo in APPtg mice. We found that bithionol and mitoxantrone but not hexachlorophene significantly reduced A β accumulation and neurodegenerative pathology in APPtg mice by stabilizing diffuse-like plaques and reducing the levels of A β intermediates and higher order species. Moreover, the levels of amyloid deposition and the neuro-inflammatory response, as exemplified by the levels of astrogliosis, were significantly reduced.

758 Another interesting finding of our study was that although the three compounds showed similar effects in vitro, the most significant effects on reducing A β -related pathology in vivo were observed with mitoxantrone and bithionol. Mitoxantrone is an anthracenedione-derived antineoplastic agent that has also been used for the treatment of multiple sclerosis. Mitoxantrone has a MW of 444, a clogP of 2.29 and a logBB of -1.9 ; it has been shown in vitro to inhibit B-cell, T-cell and macrophage proliferation and impair antigen presentation as well

as interfere with the secretion of interferon gamma (IN- γ), TNF α and IL-2. Mitoxantrone, a DNA-reactive agent that intercalates into DNA through hydrogen bonding, causing crosslinks and strand breaks, also interferes with RNA; it is a potent inhibitor of topoisomerase II, an enzyme responsible for uncoiling and repairing damaged DNA.

In contrast, bithionol is a halogenated bisphenol with a MW of 370, a logP of 5.72 and a logBB of $+0.34$ that has been used as a local anti-infective and anti-platyhelminthic agent. The mechanisms for its anti-infective actions are not well understood. Hexachlorophene is similar to bithionol and is a chlorinated version of a bisphenol with an antiseptic and bacteriostatic action against Gram-positive organisms, but is substantially less effective against Gram-negative organisms. The antiseptic mechanism of action occurs by inhibiting the membrane-bound portion of the electron transport chain, respiratory D-lactate dehydrogenase, thus blocking cellular respiration. Hexachlorophene has a MW of 371, a clogP of 6.39 and a logBB of $+0.50$. Bithionol has not been tested in AD models; however, recent studies have shown that this compound is a robust activator of Slack channels. The Slack (sequence like a calcium-activated K channel) (Slo2.2) gene is abundantly expressed in the mammalian brain and encodes a sodium-activated K⁺ (KNa) channel. Although the specific roles of Slack channel subunits in neurons remain to be identified, they may play a role in the adaptation of the firing rate and in protection against ischemic injury (Yang et al., 2006).

Although hexachlorophene has better parameters for trafficking into the CNS, both mitoxantrone and bithionol displayed more robust effects with respect to reducing pathology in APPtg mice, suggesting that the differences in activity for these compounds are unrelated to CNS exposure. Hexachlorophene has been shown to be neurotoxic in rats by inhibiting brain succinate dehydrogenase (SDH) activity, thus inducing spongiosis and brain edema (Kinosita et al., 2000). Hexachlorophene has not been tested before in models of neurodegenerative disorders. In contrast, mitoxantrone has been used in multiple sclerosis and has been shown to modulate the expression of Tau by interfering with the mRNA stem loop structure (Liu et al., 2009). Our results are consistent with previous studies showing that mitoxantrone can block A β oligomerization and fibril formation (Colombo et al., 2009). These compounds represent a proof of concept that inhibiting the seeding aggregation pathway might be a potential therapeutical value and provide a starting point for the development of promising anti-amyloidogenic drugs for the treatment of AD. However the compounds need to be further refined and developed to reduce the reported toxic effects.

Anatomical analysis of the pathological A β deposition in AD brains showed that A β aggregate deposition followed a hierarchical distribution (Thal et al., 2002), suggesting spreading of the aggregates during disease progression. AD brain and aged APPtg mouse brain extracts injected in young APPtg mice induced β -amyloidosis not only at the injection site but also in other brain areas. Spreading of the A β deposits was observed from the hippocampus region, i.e., the injection site, progressively to the dorsal lateral geniculate nucleus, the corpus callosum, the entorhinal cortex and in vasculatures of the thalamus and the pia mater (Eisele et al., 2009); this effect followed a template prion-like spreading mechanism (Aguzzi et al., 2007). Recent studies have shown that amyloid proteins can also spread in PD (Luk et al., 2012; Volpicelli-Daley et al., 2011; Lee et al., 2011) and Huntington's disease (Lee et al., 2011). Together, these data showed an important role for the spreading in the progression of neurodegenerative disease, and suggest blocking the spreading mechanism in AD, as in other neurodegenerative disorders, could represent a new therapeutic avenue (Lee et al., 2011).

In summary, utilizing novel in vitro assays, we identified novel compounds (mitoxantrone and bithionol) that inhibit A β seeding-mediated aggregation in vitro and demonstrated that these compounds block the A β -associated pathology in APPtg mice. Our in vitro studies suggest that the neuroprotective effects of these compounds are not mediated by their effects on APP processing or A β production, but instead by their ability to act at multiple steps on the amyloid cascade pathway, including the inhibition of A β seeding-mediated aggregation and aggregation-

mediated toxicity. It is likely that interfering with fibril growth and seeding-mediated aggregation will also enhance the clearing of A β aggregates via other physiological clearance mechanisms. Together, our work suggests that targeting seeding-mediated aggregation has great potential for developing novel small molecule drugs to prevent A β pathology formation and/or inhibit pathology spreading and neurodegeneration at different stages of AD progression.

Q24 Supplementary data to this article can be found online at <http://dx.doi.org/10.1016/j.nbd.2014.08.017>.

Q25 Uncited reference

Wouglis et al., 2005

Acknowledgments

Q26 This work is supported by the Swiss Federal Institute of Technology, Lausanne (HAL), the Strauss Foundation (HAL, SE, SD) and the NIH grants AG18440, AG022074, AG031097, and AG010435 (to EM). We would like to express our gratitude to Nathalie Jordan, John Perrin and Amy Paulino for their outstanding technical support and Abid Oueslati for assistance in preparing Supplemental Fig. S1.

References

- Aguzzi, A., Heikenwalder, M., Polymenidou, M., 2007. Insight into prions strains and neurotoxicity. *Nat. Rev. Mol. Cell Biol.* 8 (7), 552–561 (Review).
- Autiero, I., Saviano, M., Langella, E., 2013. In silico investigation and targeting of amyloid β oligomers of different size. *Mol. Biosyst.* 9 (8), 2118–2124.
- Cacquevel, M., Aeschbach, L., Osenkowski, P., Li, D., Ye, W., Wolfe, M.S., Li, H., Selkoe, D.J., Fraering, P.C., 2008. Rapid purification of active gamma-secretase, an intermembrane protease implicated in Alzheimer's disease. *J. Neurochem.* 104, 210–220.
- Colombo, R., Carotti, A., Catto, M., Racchi, M., Lanni, C., Verga, L., Caccialanza, G., De Lorenzi, E., 2009. CE can identify small molecules that selectively target soluble oligomers of amyloid beta protein and display antifibrillogenic activity. *Electrophoresis* 30, 1418–1429.
- Di Giovanni, S., Eleuteri, S., Paleologou, K.E., Yin, G., Zweckstetter, M., Carrupt, P.A., Lashuel, H.A., 2010. Entacapone and tolcapone, two catechol O-methyltransferase inhibitors, block fibril formation of alpha-synuclein and beta-amyloid and protect against amyloid-induced toxicity. *J. Biol. Chem.* 285, 14941–14954.
- Duyckaerts, C., Delatour, B., Potier, M.C., 2009. Classification and basic pathology of Alzheimer's disease. *Acta Neuropathol.* 118, 5–36.
- Eisele, Y.S., Bolmont, T., Heikenwalder, M., Langer, F., Jacobson, L.H., Yan, Z.X., Roth, K., Aguzzi, A., Staufienbiel, M., Walker, L.C., Jucker, M., 2009. Induction of cerebral beta-amyloidosis: intracerebral versus systemic Abeta inoculation. *PNAS* 106 (31), 12926–12931.
- Fraering, P.C., Ye, W., LaVoie, M.J., Ostaszewski, B.L., Selkoe, D.J., Wolfe, M.S., 2005. Gamma-secretase substrate selectively can be modulated directly via interaction with a nucleotide-binding site. *J. Biol. Chem.* 280, 41987–41996.
- Frost, B., Diamond, M.I., 2010. Prion-like mechanism in neurodegenerative diseases. *Nat. Rev. Neurosci.* 11 (3), 155–159.
- Goate, A., Chartier-Harlin, M.C., Mullan, M., Brown, J., Crawford, F., Fidani, L., Giuffra, L., Haynes, A., Irving, N., James, L., Mant, R., Newton, P., Rooke, K., Roques, P., Talbot, C., Pericak-Vance, M., Roses, A., Williamson, R., Rossor, M., Owen, M., Hardy, J., 1991. Segregation of a missense mutation in the amyloid precursor protein gene with familial Alzheimer's disease. *Nature* 349, 704–706.
- Gurlo, T., Ryazantsev, S., Huang, C.J., Yeh, M.W., Reber, H.A., Hines, O.J., O'Brien, T.D., Glade, C.G., Butler, P.C., 2010. Evidence for proteotoxicity in beta cells type 2 diabetes: toxic islet amyloid polypeptide oligomers form intracellularly in the secretory pathway. *Am. J. Pathol.* 176, 861–869.
- Harper, J.D., Lansbury Jr., P.T., 1997. Model of amyloid seeding in Alzheimer's disease and scrapie mechanistic truths and physiological consequences of the time-dependent solubility and amyloid proteins. *Ann. Rev. Biochem.* 66, 385–407.
- Hartley, D.M., Walsh, D.M., Ye, C.P., Diehl, T., Vasquez, S., Vassilev, P.M., Teplow, D.B., Selkoe, D.J., 1999. Protofibrillar intermediates of amyloid β -protein induce acute electrophysiological changes and progressive neurotoxicity in cortical neurons. *J. Neurosci.* 19, 8876–8888.
- Jan, A., Hartley, D.M., Lashuel, H.A., 2010. Preparation and characterization of toxic Abeta aggregates for structural and functional studies in Alzheimer's disease research. *Nat. Protoc.* 5 (6), 1186–1209.
- Jucker, M., Walker, L.C., 2011. Pathogenic protein seeding in Alzheimer's disease and other neurodegenerative disorders. *Ann. Neurol.* 70, 532–540.
- Kane, M.D., Lipinski, W.J., Callahan, M.J., Bian, F., Durham, R.A., Schwarz, R.D., Roher, A.E., Walker, L.C., 2000. Evidence for seeding of beta-amyloid by intracerebral infusion of Alzheimer brain extracts in beta-amyloid precursor protein-transgenic mice. *J. Neurosci.* 20 (10), 3606–3611.
- Kinosita, Y., Matsumura, H., Yokota, A., 2000. Hexachlorophene-induced brain edema in rat observed by proton magnetic resonance. *Brain Res.* 873, 127–130.
- Kraszpulski, M., Soininen, H., Helisalmi, S., Alafuzzoff, I., 2001. The load and distribution of beta-amyloid in brain tissue of patients with Alzheimer's disease. *Acta Neurol. Scand.* 103, 88–92.
- Kumar-Singh, S., Theuns, J., Van Broeck, B., Pirici, D., Vennekens, K., Corsomiu, E., Cruts, M., Dermaut, B., Wang, R., Van Broeckhoven, C., 2006. Mean age-of-onset of familial Alzheimer's disease caused by presenilin mutations correlates with both increased A β_{42} and decreased A β_{40} . *Hum. Mutat.* 27, 686–695.
- Langer, F., Eisele, Y.S., Fritsch, S.K., Staufienbiel, M., Walker, L.C., Junker, M., 2011. Soluble A β are potent inducers of cerebral β -amyloid. *J. Neurosci.* 31, 14488–14495.
- Lee, S.J., Desplats, P., Sigurdson, C., Tsigelny, I., Masliah, E., 2010. Cell-to-cell transmission of non prion protein aggregates. *Nat. Rev. Neurosci.* 6, 702–706.
- Lee, S.J., Lim, H.-S., Masliah, E., Lee, H.-J., 2011. Protein aggregate spreading in neurodegenerative diseases: problems and perspectives. *Neurosci. Res.* 70, 339–348.
- Lemere, C.A., Blusztajn, J.K., Yamaguchi, H., Wisniewski, T., Saido, T.C., Selkoe, D.J., 1996. Sequence of deposition of heterogeneous amyloid beta peptides and APOE in Down syndrome: implications for initial events in amyloid plaque formation. *Neurobiol. Dis.* 3, 79–84.
- Lesne, S., Koh, M.T., Kotilinek, L., Kaye, R., Glabe, C.G., Yang, A., Gallagher, M., Ashe, K.H., 2006. A specific amyloid-beta protein assembly in the brain impairs memory. *Nature* 440, 352–357.
- Lewis, J., Dickson, D.W., Lin, W.L., Chisholm, L., Corral, A., Jones, C., Yen, S.H., Sahara, N., Skipper, L., Yager, D., Eckman, C., Hardy, J., Hutton, M., McGowan, E., 2001. Enhanced neurofibrillary degeneration in transgenic mice expressing mutant tau and APP. *Science* 293, 1487–1491.
- Liu, Y., Peacey, E., Dickson, J., Donahue, C.P., Zheng, S., Varani, G., Wolfe, M.S., 2009. Mitoxantrone analogues as ligands for a stem-loop structure of tau pre-mRNA. *J. Med. Chem.* 52, 6523–6526.
- Luk, K.C., Kehm, V.M., Zhang, B., O'Brien, P., Trojanowski, J.Q., Lee, V.M., 2012. Intracerebral inoculation of pathological α -synuclein initiates a rapidly progressive neurodegeneration α -synucleinopathy in mice. *J. Exp. Med.* 209, 975–986.
- Masliah, E., Rockenstein, E., Veinbergs, I., Mallory, M., Hasimoto, M., Takeda, A., Sagara, Y., Sisk, A., Mucke, L., 2000. Dopaminergic loss and inclusion body formation in alpha-synuclein mice: implications for neurodegenerative disorders. *Science* 287, 1265–1269.
- Masliah, E., Rockenstein, E., Veinbergs, I., Sagara, Y., Mallory, M., Hashimoto, M., Mucke, L., 2001. β -Amyloid peptides enhance α -synuclein accumulation and neuronal deficits in a transgenic mouse model linking Alzheimer's disease and Parkinson's disease. *PNAS* 98, 12245–12250.
- McLean, C.A., Cherny, R.A., Fraser, F.W., 1999. Soluble pool of A-beta amyloid as a determinant of severity of neurodegeneration in Alzheimer's disease. *Ann. Neurol.* 46, 860–866.
- Meyer-Luehmann, M., Coomaraswamy, J., Bolmont, T., Kaeser, S., Schaefer, C., Kilger, E., Neuenschwander, A., Abramowski, D., Frey, P., Walsh, D.M., Mathews, P.M., Ghiso, J., Staufienbiel, M., Walker, L.C., Jucker, M., 2006. Exogenous induction of cerebral beta-amyloidogenesis is governed by agent and host. *Science* 313 (5794), 1781–1784.
- Mucke, L., Masliah, E., Yu, G.Q., Mallory, M., Rockenstein, E.M., Tatsuno, G., Hu, K., Kholondeko, D., Jhonson-Wood, K., McConlogue, L., 2000. High-level neuronal expression of A beta 1–42 in wild-type human amyloid protein precursor transgenic mice: synaptotoxicity without plaque formation. *J. Neurosci.* 20, 4050–4058.
- Nilsberth, C., Westlind-Danielsson, A., Eckman, C.B., Condron, M.M., Axelman, K., Forsell, C., Stenh, C., Luthman, J., Teplow, D.B., Younkin, S.G., Naulund, J., Lannfelt, L., 2001. The Arctic APP mutation (E693G) causes Alzheimer's disease by enhanced A β protofibril formation. *Nat. Neurosci.* 4, 887–893.
- Pham, E., Crews, L., Ubhi, K., Hansen, L., Adame, A., Cartier, A., Salmon, D., Galasko, D., Michael, S., Savas, J.N., Yates, J.R., Glabe, C., Masliah, E., 2010. Progressive accumulation of amyloid- β oligomers in Alzheimer's disease and in amyloid precursor protein transgenic mice is accompanied by selective alterations in synaptic scaffold proteins. *FEBS J.* 272, 3051–3067.
- Rockenstein, E., Mallory, M., Mante, M., Sisk, A., Masliah, E., 2001. Early formation of mature amyloid- β protein deposits in a mutant APP transgenic model depends on levels of A β_{1-42} . *J. Neurosci. Res.* 66, 573–582.
- Rockenstein, E., Mallory, M., Alford, M., Windisch, M., Moessler, H., Masliah, E., 2002. Effects of cerebrolysin on amyloid-beta deposition in a transgenic model of Alzheimer's disease. *J. Neural Transm. Suppl.* 62, 327–336.
- Selkoe, D.J., 2012. Alzheimer's disease: genes, proteins and therapy. *Physiol. Rev.* 81, 741–766.
- Sthor, J., Watts, J., Mensiger, Z.L., Oehler, A., Grillo, S.K., Dearmond, S.J., Prusiner, S.B., Giles, K., 2012. Purified and synthetic Alzheimer's amyloid beta prions. *PNAS* 109 (27), 11025–11030.
- Sturchler-Pierrat, C., Staufienbiel, M., 2000. Pathogenic mechanisms of Alzheimer's disease analyzed in the APP23 transgenic mouse model. *Ann. N. Y. Acad. Sci.* 920, 134–139.
- Thal, D.R., Rub, U., Orantes, M., Braak, H., 2002. Phases of amyloid- β -deposition in the human brain and its relevance for the development of AD. *Neurology* 58 (12), 1791–1800.
- Volpicelli-Daley, L.A., Luk, K.C., Patel, T.P., Tanik, S.A., Riddle, D.M., Stieber, A., Meaney, D.F., Trojanowski, J.Q., Lee, V.M., 2011. Exogenous α -synuclein fibrils induce Lewy body pathology leading to synaptic dysfunction and neuron death. *Neuron* 72, 57–67.
- Walker, L.C., Diamond, M.I., Duff, K.E., Hyman, B.T., 2013. Mechanism of protein seeding in neurodegenerative disease. *JAMA Neurol.* 70 (3), 304–310.
- Wouglis, M., Wright, S., Cunningham, D., Chilcote, T., Powell, K., Rydel, R.E., 2005. Nucleation-dependent polymerization is an essential component of amyloid-mediated neuronal cell death. *J. Neurosci.* 25 (5), 1071–1081.
- Yang, B., Gribkoff, V.K., Pan, J., Damagnez, V., Dworetzky, S.I., Boissard, C.G., Bhattacharjee, A., Yan, Y., Sigworth, F.J., Kaczmarek, L.K., 2006. Pharmacological activation and inhibition of Slack (Sl α 2) channels. *Neuropharmacology* 51, 896–906.